β

CONDENSATION OF AMMONIA VAPOR DURING RAPID EXPANSION

MICHAEL KREMMER

OLUFEMI OKUROUNMU

D D C

FEB 1 8 1965

DDC-IRA   E
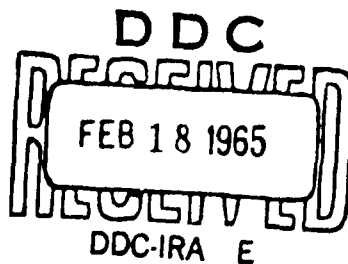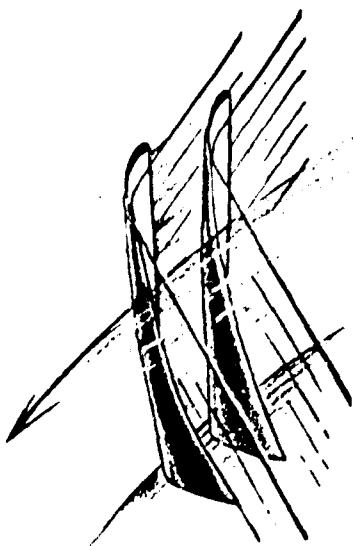
January, 1965

GAS TURBINE LABORATORY
MASSACHUSETTS INSTITUTE OF TECHNOLOGY
CAMBRIDGE · 39 · MASSACHUSETTS

CONDENSATION OF AMMONIA VAPOR

DURING RAPID EXPANSION

by

MICHAEL KREMMER & OLUFEMI OKUROUNMU

GAS TURBINE LABORATORY

REPORT No. 79

January 1965

MASSACHUSETTS INSTITUTE OF TECHNOLOGY

Cambridge, Massachusetts

ABSTRACT

This report presents an experimental study, through pressure distributions, of the homogeneous nucleation and condensation of initially superheated ammonia vapor during its expansion in a low Mach number supersonic nozzle. The results of the experiments are compared with the classical nucleation theory of Becker and Doring or Frenkel-Zeldovich, on the basis of the predicted pressure and temperature at which condensation would occur starting from a given stagnation condition.

It is found that ammonia shows far less supersaturation than this theory predicts. The effect of arbitrary corrections to the surface tension showed that a further reduction in surface tension of the drop relative to the flat-film value gives better agreement between measured and predicted pressure distributions. Even better agreement is obtained without a surface tension correction if we assume that the nucleation rate is greater by a factor of 10^{17}. This seems to lend some support to the recent theories of Lothe and Pound[28] and Oriani and Sundquist[30] concerning gassification corrections to the free energy of formation of critical droplets. It is not certain however how much of this correction can be assigned to uncertainties in surface tension, and how much to the 'gassification' effect.

ACKNOWLEDGEMENTS

TABLE OF CONTENTS

LIST OF FIGURES

NOMENCLATURE

a	velocity of sound in the vapor
A	cross-section area
A^*	throat area
$\bar{A}$	molecular weight
C	specific heat of the liquid
c_p	specific heat of the vapor at constant pressure
c_v	specific heat of the vapor at constant volume
f_g	number of g-sized drops
g	earth acceleration
g	number of molecules in a droplet
g^*	critical number of molecules in a droplet
h	enthalpy
h_{fg}	enthapy change due to condensation
I	nucleation rate per unit volume
I_{cr}	critical nucleation rate per unit volume
k	Boltomann's molecular gas constant
K_E	Eötvös constant
m	mass of a molecule
$\dot{m}$	mass flow
M	Mach number
N_g	distribution of g-sized drops
N_o	Avogadro's number
p	pressure
$p_\infty, p_{g\infty}$	flat film saturation pressure
Q	heat per unit mass
r	drop radius
(r)	average drop radius

r^*	critical drop radius
r_o	radius of smallest, newly-built drops
r_M	molecular radius
R	gas constant
s	entropy
S	surface of all drops passing the nozzle area per unit time
S_g	surface of a g-sized drop
t	time
t, T	temperature
T_K	critical temperature
u	internal energy
U_{fg}	change of internal energy due to condensation
v, v_B	volume of a liquid molecule
v	specific volume of vapor
F	velocity
x	length along nozzle
y	$= \sigma/r^*$
$z, z1$	helpful variables to solve equations (37)
α_g	number of molecules evaporated from a g-sized drop per unit time per unit area
β	number of molecules striking unit drop surface per unit time
δ	correction in surface tension
δ^*	boundary layer displacement thickness
θ	boundary layer momentum thickness
ξ	condensation coefficient
κ	isentropic exponent
λ	$= h_{fg}/c_p \cdot T$

μ	liquid mixture mass ratio
ρ	density
σ	surface tension
σ_∞	flat film surface tension
ϕ	Gibbs free energy

Subscripts

A, g or none	properties of the vapor
B or L	properties of the liquid
D	conditions inside the drops
g or (g+1)	properties for g or (g+1)-sized drops
s	isentropic process
0	stagnation conditions before the nozzle

CONDENSATION OF AMMONIA VAPOR DURING RAPID EXPANSION

by

Michael Kremmer & Olufemi Okurounmu

I. INTRODUCTION

A. Background to the Problem

Interest in the phenomenon of condensation of vapors undergoing various forms of expansion have gained considerable momentum amongst scientists and engineers over the last few decades. However, the state of knowledge in this field over the same period has improved, if at all, by very little and is at the moment in a rather unsatisfactory condition. This is not to say that no progress has been made, indeed, several heretofore unrecognized factors that do have a significant influence on condensation have now been emphasized by recent investigators, but to the extent that there is not in general a consensus of expert opinion on the exact nature of the interrelationships between these variables, the role of experiments cannot be over-emphasized, more or less as an arbiter between the various existing theories of nucleation.

By condensation, in this report, we refer to that resulting from homogeneous nucleation from the vapor phase, the nuclei in this case being clusters of atoms of the vapor which increase in number as the supersaturation of the vapor increases, and subsequently cause a collapse of the supersaturated state.

Some of the earliest experiments on this phenomenon were conducted by Wilson[1]. Powell[2] and later by Volmer and Flood[3], all utilizing cloud chambers for the expansion, although a few earlier nozzle experiments had been done by Hirn and Cazin[27]. It is well known however that a cloud chamber expansion is inherently an unsteady process, is very much influenced by the presence of dust or any other foreign particles, since the expansion

rate is very slow and hence allows considerable interaction between the dust particles and the vapor. Besides, observation of condensation in cloud chamber experiments depends on visual observation of the appearance of a cloud, whereas Hill[4], by comparing Yellot's separate measurements of visible cloud and pressure distributions, has concluded that the actual appearance of visible clouds occurs a little later than the beginning of condensation. Since the entire process is unsteady, it is impossible to obtain a history of the events prior to condensation. One could, therefore, wonder whether cloud chamber data can truly be used to check existing nucleation theories, mostly based on the assumption of a steady state distribution of nuclei; and one might say that any apparent agreement between theory and data obtained from cloud chambers would at least be partly fortuitous and would not truly reflect the validity of the theory itself.

Other experimenters have studied the same phenomenon through nozzle expansions, using superheated steam as the vapor. The data of Stodola[5], Yellot[6],[7] Retalliata[8], Binnie and Woods[9], and those of Wegener & Pouring[16] are well-known in the literature. Nozzle expansions are no doubt more reliable than cloud chamber expansions; steady state can very readily be maintained, and because of the very high expansion rates, dust particles cannot have any appreciable effect on nucleation. It has been shown by Oswatitsch[10] that dust particles with a concentration of as high as 10^8 particles per cc. would have virtually no effect on the condensation of steam in a nozzle. The nozzle data mentioned above compares favourably with the Becker-Doring equation, as shown by Hill[4]. But, since all the available data in the literature is on steam, it would seem that a true test of existing theories cannot be made until reliable data on other vapors becomes available. It is with this in mind that the present experiments have been conducted. It is hoped that it will supplement existing data on steam in enabling us to determine just how useful existing theories are in 1) pre-

dicting the onset of condensation, and 2) describing the history of the condensation, particularly in terms of pressure distributions in the vapor, both before and after the actual condensation process.

It will not be out of place at this point to ask just why there is a need for a better understanding of such a simple process as condensation in a vapor? While the physicist or chemist may be interested for quite different reasons, the engineer is primarily concerned with the effects of possible condensation of the working fluid in a power plant on the cycle efficiency and other design parameters. Since, in the Rankine cycle with saturated vapor at the turbine inlet, condensation of the working fluid is almost inevitable, a good design would have to take this into consideration, by making allowance for losses due to a) the drag of the condensed droplets and b) drop inpingement on successive rows of blades. The exit area required to pass a given flow would also have to be greater if condensation occurs in the working fluid.

B. Nucleation Theory

There have been several forms of the nucleation rate equation developed by various authors, outstanding among whom are Volmer and Weber[12], Becker and Doring[13] and Zeldovich[14]. An outline of the derivation, together with the necessary assumptions is presented below, along the lines of Frenkel, Becker, and Doring[13], [15].

It is assumed that:

1) there are present in the vapor, at any instant of time, microscopic embryos of the liquid phase, with varying sizes acting as nuclei, and differing from the macroscopic state of the liquid only in their size.

2) The thermodynamic state of these embryos may be described by macroscopic properties of the liquid phase, even though they contain, in general, only a few molecules.

3) The energy of formation of the embryo consists of two sums: a) the Gibbs free energy change associated with the condensation of bulk liquid from the vapor phase, and b) the surface energy associated with the comminution of the bulk liquid into spherical droplets.

Thus, the free energy change in the formation of a g-sized drop is given by

$$\Delta \bar{\Phi} = (\phi_B - \phi_A)g + 4\pi r^2 \sigma$$

where ϕ_B = Gibbs free energy/molecule in the liquid phase

ϕ_A = Gibbs free energy/molecule in the gaseous phase

g = number of molecules in the drop

σ = surface tension of liquid

We define

$$\mu g^{2/3} = 4\pi r^2 \sigma \qquad (1)$$

Then
$$\Delta \bar{\Phi} = (\phi_B - \phi_A)g + \mu g^{2/3} \qquad (2)$$

It is seen that $\Delta \bar{\Phi}$ has a maximum value at

$$g = g^* = \left(\frac{2}{3} \frac{\mu}{\phi_A - \phi_B}\right)^3 \qquad (3)$$

where g^* is defined as a critical sized embryo, being the size that involves the greatest change in free energy, and hence, most difficult to form.

For a stable vapor for which ($\phi_A < \phi_B$), as opposed to a supersaturated one ($\phi_A > \phi_B$), the steady distribution of embryos is given by the Boltzman distribution:

$$N_g = Ce^{-\Delta \bar{\Phi}/kT} \qquad (4)$$

We then assume, that even for the case $\phi_A > \phi_B$, this same distribution may be used, and thus obtain

$$N_{g^*} = Ce^{-\Delta \bar{\Phi}_{max}/kT} \qquad (5)$$

where C roughly equals the total number of molecules in the system.

From (1), (2) and (3)

$$\Delta \bar{\Phi}_{max} = \frac{4\pi}{3} \sigma r^{*2} \qquad \text{where } r = r^* \qquad \text{when } g = g^*$$

The distribution (5) shows Ng* to correspond to the minimum value of Ng. Use of this distribution assumes that there are no mutual interactions between the various embryos, which can therefore be treated as if they were isolated from one another.

After writing the appropriate expressions for ϕ_A, ϕ_B, in (2), differentiation at fixed $(T = T_D)$, with $\frac{d(\Delta\bar{\phi})}{dg} = 0$, and assuming $v_B \ll v_A$, gives

$$\ln \frac{p}{p_\infty} = \frac{2\sigma v_B}{r^* kT} = \frac{2\sigma}{\rho_L R T_D r^*} \tag{6}$$

where v_B = volume/molecule in liquid phase

   R = gas constant

   T_D = temperature of liquid drop

From here on, we further assume that:

1) All drops of a certain size $G > g^*$ are eliminated from the system and replaced by an equivalent number (GN_G) of single molecules.

Thus the number of drops of any size remain constant. Hence, if

   α_g = number of molecules evaporated from the surface of a g-sized drop/unit time/unit area

   β = number of molecules striking unit drop surface/unit time.

This assumption requires that:

$$N_g S_g \alpha_g = N_{g-1} S_{g-1} \beta \tag{7}$$

β is given from kinetic theory as:

$$\beta = \frac{p}{\sqrt{(2\pi m kT)}} \tag{8}$$

and S_g = surface area of a g-sized drop. For $g \gg 1$, it is a good assumption that $S_{g-1} \approx S_g$.

Hence, substitution for N_g, N_{g-1} from (5) in (7) gives the result:

$$\alpha_g = \beta e^{(1/kT)(\phi_B - \phi_A + 2\sigma v_B/r_g)} \tag{9}$$

We see that, for $g = g^*$

$$\alpha_{g^*} = \beta$$

We now assume that α_g as given in (9) holds even for a non-equilibrium distribution of embryo sizes, and proceed to determine the rate of change from a non-equilbrium distribution characterized by f_g. Taking account of condensation on, and evaporation from the drop, we define I_g as:

$$I_g = f_{g-1} S_{g-1} \beta - f_g S_g \alpha_g \qquad (10)$$

equals rate of formation of g-sized drops due to condensation on (g-1) sized drops and evaporation of g-sized drops. Similarly,

$$I_{g+1} = f_g S_g \beta - f_{g+1} S_{g+1} \alpha_{g+1} \qquad (11)$$

equals rate of decay of g-sized drops due to condensation on g-sized drops and evaporation of (g+1) sized drops.

Hence, net rate of formation of g-sized drops is given from (10) and (11) as:

$$\partial f_g / \partial t = I_g - I_{g+1} \qquad (12)$$

In steady state $\partial f_g / \partial t = 0$.

For $g \gg 10$, f_g can be treated as a function of a continuous variable, g, and $(I_g - I_{g+1})$ replaced by $-\partial I / \partial g$.

The appropriate boundary condition is that at $g = G$, $f(g) = 0$, and an approximate solution of (12) can be expressed as

$$I = (P/kT)^2 \upsilon \sqrt{(2\sigma/\pi m)} \exp(-4\pi\sigma r^{*2}/3kT)$$

where the further assumption has been made that I is independent of g for $g < g^*$, and r^* is given by (6).

Certain modifications to this theory have recently been suggested by Lothe and Pound[28] who have pointed out additional terms which should be inlcuded in the free energy of formation of critical nuclei as mentioned above:

a) They believe that errors due to assigning macroscopic properties to the embryo may be reduced by taking account of the entropy reduction accompanying the separation of say, g molecules from a larger liquid bulk of gN_g molecules. This would add to the free energy of

formation of critical sized embryos, a term $\Delta \Phi_I = kT \ln(2\pi g)/2$, and lead to a consequent reduction in the equilibrium distribution of critical nuclei of an order of magnitude

b) Since 6 degrees of freedom are required to energize the embryos, conservation of degrees of freedom requires that 6 degrees of freedom in the individual molecules be de-activated. This leads to a further increase $\Delta \Phi$ given by

$$\Delta \Phi_{II} = + TS$$

and hence, to a decrease in the equilibrium concentration of critical nuclei by a factor of about 10^{-2}.

c) The embryos also have 3 translational degrees of freedom and a certain translational energy associated with these, which lead to a decrease in $\Delta \Phi_{max}$ given by

$$\Delta \Phi_{III} = - kT \ln \left[(2\pi m kT)^{3/2} \Omega / h^3 \right]$$

where m = molecular mass of embryo,

Ω = molecular volume of embryo in gaseous state at P, T. For water vapor, this is of the order of $- 24\ kT$ when $g^* \approx 100$ molecules, and leads to an increase in I by a factor of about 10^{11}.

d) The rotational degrees of freedom of the embryos also contribute to the energy and entropy of formation of critical nuclei. Assuming the molecules in the embryo to be rigid, and the droplet spherical, so that $(I_1 = I_2 = I_3 = I$ = moment of inertia), we obtain a further contribution to $\Delta \Phi_{max}$ given by

$$\Delta \Phi_{IV} = - kT \ln \left[(2kT)^{3/2} (\pi I^3)^{1/2} h^3 \right]$$

which is roughly $= - 21\ KT$ for water vapor droplets with $g^* = 100$ at $300\ °K$; and increases I by a factor of about 10^9.

Summing the factors (a) to (d), we have

$$\Delta \Phi_I + \Delta \Phi_{II} + \Delta \Phi_{III} + \Delta \Phi_{IV} \approx - 45\ kT$$

for water droplets, corresponding to an increase in the distribution of critical nuclei by a factor of roughly 10^{20}.

More recently, Oriani and Sundquist[30], by similar considerations to the above, have arrived at a correction factor of about 10^{18} for water vapor; and Courtney[19], [29] following the 'conservation-of-degrees-of-freedom-approach', has come up with correction factors of about 10^{4}, 10^{6}, and 10^{9} for monatomic, linear and non-linear polyatomic condensing molecules, respectively.

Further Growth of the Drops[5, 10]

The growth rate of the drops is obtained by considering mass transfer between vapor and droplets. Let ξ = the fraction of molecules striking a drop surface that condense on it. The mass flux from the drop equals mass flux to it from an environmental condition T_D, P_D, corresponding to drop temperature and pressure. With β defined by (8) the mass flux from the drop surface,

$$= \xi P_D \big/ \sqrt{2\pi R T_D}$$

where P_D = saturation pressure corresponding to drop temperature, T_d. But mass flux to the surface of the drops

$$= \xi P \big/ \sqrt{2\pi R T}$$

$\therefore$ By continuity:

$$\rho_L 4\pi r^2 dr/dt = 4\pi r^2 \left[\frac{\xi P}{\sqrt{2\pi R T}} - \frac{\xi P_D}{\sqrt{2\pi R T_D}} \right]$$

or

$$\frac{dr}{dt} = \frac{\xi}{\sqrt{2\pi}\rho_L} \left[\frac{P}{\sqrt{RT}} - \frac{P_D}{\sqrt{RT_D}} \right] \tag{13}$$

The drop temperature is calculated by a balance of energy gluxes. We assume an accommodation coefficient of 1, which implies that all of the energy associated with molecules striking a drop surface is reflected, at the temperature corresponding to T_D. These considerations lead to the expression

$$r C \big/ 3 U_{fg} \frac{dT_D}{dt} = \frac{dr}{dt} - \frac{3}{2\sqrt{2\pi} U_{fg}\rho_L} \frac{P}{\sqrt{RT}} \left[RT_D - RT \right] \tag{14}$$

It is found that $dT_D/dt \gg dr/dt$, and hence we may assume $T_D = T_D(r)$.

Eliminating dr/dt from (13), (14), plus use of (6) yields:

$$\frac{2}{3} \frac{U_{fg} \xi}{RT} \left[1 - \frac{P_{s\infty}}{P} exp \left\{ \frac{2\sigma}{\rho_L R T_D r} \right\} \sqrt{\frac{T}{T_D}} \right] = \frac{T_D}{T} - 1 \quad (15)$$

II. EXPERIMENTAL WORK

A. Preliminary Considerations

It was desirable for experimental purposes to choose a test fluid which condenses with marked property changes and which would therefore render the detection of condensation fairly easy. This purpose would be adequately served by a fluid which first has a high nucleation rate, and which, from a given stagnation condition, approaches saturation rapidly since it is desirable to have condensation at fairly low Mach numbers. An examination of the nucleation rate equation shows it to be strongly dependent on the exponential index, and hence, a useful parameter of nucleation rate might be taken as $K_1 = \frac{\sigma^3}{\rho_L^2 R^2}$. A low value of this parameter would indicate a very high tendency to form condensation nuclei very rapidly. The second requirement of rapid approach to saturation is governed by the parameter $K_2 = \frac{h_{fg}}{C_p T}$ obtained from gas-dynamic considerations. A better grasp of its actual significance is obtained from the following illustration[17].

The Clausis-Clapeyron Equation gives, along the saturation curve:

$$\frac{dP_\infty}{dT} = \frac{h_{fg}}{v_g T} = P h_{fg}/RT^2 \quad (16)$$

For isentropic expansion,

$$\left(\frac{dP}{dT}\right)_s = \frac{P}{T} \cdot \frac{\kappa}{\kappa - 1} \quad (17)$$

Hence,

$$\left(\frac{dP_\infty}{dT}\right) / \left(\frac{dP}{dT}\right)_s = h_{fg}/c_p T \quad (18)$$

For high values of $h_{fg}/C_p T$ the saturation line is much steeper than the isentropes, and hence, for decreasing temperature along a given isentrope, rapid approach to the saturation line is achieved. Typical values of the two parameters for ammonia, and a few other vapors are listed below for comparison.

Table I.

	$\dfrac{\sigma^3}{\rho_L{}^2 R^2}$	$\dfrac{h_{fg}}{c_p T}$	$T\ ^\circ R$
Ammonia	.3	2.5	456
Freon 12	1.3	1.4	470
H_2O	1	2.8	706
Mercury	196	4.5	920

normalized with $H_2O = 1$

Comparison of Condensation Parameters for a Few Fluids

Initial estimates of the boundary layer thickness at the throat of a converging passage, assuming a linearly increasing velocity, and a reasonably arbitrary initial momentum thickness, θ_o , were made as a guide towards the selection of a nozzle geometry which would truly justify neglecting boundary layer corrections. The calculations show that the assumed θ_o is relatively insignificant. The method used was that of Launder[18], in which effects of compressibility of the fluid were neglected. The calculated δ^*/D at the throat of the nozzle was of the order of 1%.

B. Apparatus and Experimental Procedure

The complete schematic of the Apparatus is shown in Figure 1, with more details shown in Figures 2. Ammonia is taken from the tank, A, where it exists in equilibrium with its vapor at a pressure of 114 psig and 70°F. It is then led into the boiler, B, the flow being controlled by the valve (I). The boiler consists of about 16 turns of 5/8" O.D. stainless steel tubing through which condensing steam is passed at pressures ranging from 10 to 20 psig. The ammonia flows on the outside of the coils. It was found that, with this arrangement, steady state was more easily obtained than if the flow paths of the steam and ammonia were interchanged. A sight gauge showed the level of ammonia in the boiler. As much as possible, the level was kept the same throughout an experimental run. The cyclone-action separator, C, served to remove all liquid droplets left in the vapor, after leaving the boiler. The ammonia then passes to the test section through the needle valve (II), which was used to control the stagnation pressure.

The test section consists of a stagnation tank, 6" I.D., with three perforated screens held in position by sleeves, and arranged as shown in Figure 2b. The tank is fed by about 16 turns of 5/8" O.D. aluminum tubing, and the entire assembly is immersed in a rectangular tank filled with water at various temperatures. The stagnation tank carries a pressure gauge, a thermometer and thermocouple. From the settling tank, the ammonia goes into the test nozzle, along which measurements of pressure distributions are made.

Two nozzles have been used in the tests, an axi-symmetric nozzle, shown in Figure 2b, and later a two-dimensional one. The one-dimensional design was based on the work of Wang and Co, who described a method of obtaining uniform flows at the outlet of a converging channel: with a view towards having a uniform flow at the throat. The diverging part of the nozzle was conical, although this meant having a discontinuity of curvature at the

throat. It was felt however that this could not introduce any great disturbances to the measured pressure distributions. Pressure taps, 20/1000" I.D. were located at 1/4" apart along the walls in the diverging section. The diverging part was 3" long, had a throat diameter of 2/10" and an exit diameter of 27/100". Such small dimensions were necessitated by mass flow considerations. Unfortunately, however, this nozzle did not prove very useful. First, for a nozzle of such small dimensions, the pressure taps have to be perfectly smooth and rounded off. Any small burrs or irregularities in the taps proved to have a considerable influence on the pressure distributions. Hence, after any one run, the deposited moisture usually had a disturbing effect on the taps, and the following set of pressure measurements usually differed considerably from the previous one, employing al/most identical upstream conditions. An attempt to solve this problem was made by reaming out the nozzle after every few runs, but this in itself was self-defeating, since it meant that the runs were necessarily irreproducible because of the constantly changing geometry. It was to resolve this dilemma that the two-dimensional nozzle was constructed. This is shown in Figure 3.

The inlet consists of circular arcs, with a 1" radius. The angle of divergence can be varied between about $1°$ to $4°$ total included angle. Pressure taps, 16/1000" diameter were spaced 1/4" apart near the throat, and 1/2" apart further downstream. The throat width was about 15/100" independent of divergence angle, and the nozzle height, uniform everywhere, was 1/5". The nozzle can be taken apart and cleaned between runs, a great advantage over the one-dimensional one.

The ammonia is finally discharged by dissolving it in a steady stream of cold water and leading the mixture into the drain. The air passages (Ref. Fig 1a) are provided for blowing out either the test section or the entire apparatus.

The procedure for obtaining a complete set of pressure distributions
is as follows: (ref. Fig. 1a). The water in the rectangular tank is kept
at the appropriate temperature. Steam is turned on to a suitable pressure
level, usually about 10 psig, and left tunning for about 5 minutes to warm
up the coils in the boiler. The cold water is next turned on and a steady
stream maintained, with a little overflow from the quenching tank, D. Next,
the outlet valve from the ammonia tank is opened, so that valve I experi-
ences the full tank pressure. With the needle valve II now slightly opened,
valve I is opened fairly wide, and immediately, the exhaust valve III is
opened. Fine regulation of the needle valve now gives any desired stag-
nation pressure, a rough value of which is read on the pressure gauge. The
valve III is necessary to prevent suck back of water from the quenching
tank when the system is shut off. The stagnation temperature can be varied
between two extremes, neamely, the triple point of water and the boiling
point. Initially, the water in the tank is heated electrically to near
boiling, and for subsequent runs, varying intermediate temperatures are
obtained by emptying differing amounts of the hot water, and refilling the
tank with cold water. Eventually, the water is cooled to normal cold water
temperature, from which point its temperature can be lowered still further
by adding varying amounts of ice. Strictly speaking, the intermediate
temperatures cannot be held constant, but since it takes less than 2 minutes
to take a set of pressure distributions, it is assumed that the tank temper-
ature cannot vary much in this interval. This assumption is borne out by
the experimental data.

The pressure readings are taken with a transducer, utilizing a rotary
switch device shown schematically in Figure 4. The switch consists of two
discs, the top one rotating on nylon bearings mounted axially through the
bottom one. The latter has 24 holes drilled through it circumferentially,

and each connected to a pressure tap by flexible tubing. Each pressure hole in the lower disc is individually sealed by an O-ring between the two discs, and a single search tube through the upper disc picks up the pressure in each tap as it turns around, and transmits it to the transducer. Callibration shows the transducer response to be linear with pressure. The signal is fed into an amplifier with a suitable outlet for connection to an x-y recorder. The recorder is calibrated to record the numerical values of the pressures directly.

The stagnation temperature is read simultaneously with a thermometer and a Chromel-Alumel thermocouple, both of which have been previously calibrated and found to check with each other to within $1/2^{\circ}F$.

The average mass flow in most of the runs was about 3 cu ft/hr, with stagnation pressures varying between 30 and 70 psia, and stagnation temperatures between 32° and $190^{\circ}F$.

C. Precision of the Measurements

The calibration of the transducer showed it to be linear with pressure, as illustrated in Figure 5. To allow for the possibility that the straight line might shift parallel to itself, the zero pressure point was usually checked before each set of readings. It is assumed that the gain of the d.c. amplifier does not depend on the magnitude of the excitation voltage, and hence, a linear input would also give a linear output. However, since the calibration of the amplifier output was achieved by setting the dial pointer to correspond to a known pressure from a mercury manometer, there exists two sources of uncertainty; first, in reading the manometer levels, and secondly, in setting the pointer to correspond to the known pressure. These two errors could of course be in opposite directions, and hence cancel out, but assuming they are in the same direction, and allowing an uncertainty of $\pm 0.4"$ for the mercury levels, the cumulative error could be of

the order of $\pm$ 0.7 psia. There is a third error involved in reading the recorded pressures, which can only be read conveniently to about $\pm$ 0.2 psi. Thus, the worst possible uncertainty in the pressures shown on the data may be assumed to be not greater than 0.9 or about 2%. Concerning the speed of response of the entire sensing-amplification-recording system, sufficient time was generally allowed for a flat pressure response to be obtained at a given pressure tap before switching on to the next pressure tap. The typical duration of time spent at a pressure location was about 3 seconds; during which the pressure was observed to attain a flat steady value within the first 3/4 of a second.

The accuracies regarding the temperature measurements are perhaps a little more precise. It is difficult to balance the potentiometer any closer than to within $\pm$ 0.02mv, or about $\pm$ 1°F. An additional error of $+(0\rightarrow.5)$°F may be assumed due to the reference junction not being exactly at 32°F, this being always in the positive direction. Except in a few runs, temperatures at the beginning and at the end of a run did not differ by more than 1.5°F and most of this is estimated to result from the error of balancing as mentioned earlier. The temperatures as given in the data may therefore be assumed to be accurate to within -1.0 to + 1.5°F. A further point may be made as regards the purity of the ammonia. The commercial grade that was used was certified by the manufacturer to be of 99.95% purity, containing less than 50 ppm of water vapor, and less than 5 ppm of oils and other non-condensibles[20]. The nucleation that led to the condensation may therefore be assumed homogeneous as explained earlier.

D. Experimental Results and Discussion

The upper curves in Figures 6 and 7 show the experimental pressure distributions obtained with the axisymmetric nozzle. The lower curves are, respectively, the theoretical pressure distribution, and the isentropes.

Figures 8 - 15 show the pressure distributions from the two-dimensional nozzle. The curves in each figure correspond approximately to the same stagnation pressure, but with differing stagnation temperatures. They were all obtained with a total nozzle included angle of 1°. The lowest curve corresponds to a high enough superheat of the vapor so that no condensation occurs in the nozzle. We refer to this as the 'non-condensing' curve, and use it as a reference for the other curves. Qualitatively, Figures 8 - 15 are very similar, and hence, the following remark , referred specifically to Figure 10, is applicable to all of them

1) The non-condensing curve lies in general above the isentropic curve (not shown) corresponding to the geometry of the nozzle. This is mostly due to frictional effects, resulting in an effective nozzle area different from the geometric area at any cross-section. The frictional effects are more pronounced in the supersonic section of the nozzle than in the subsonic part. For the same reason, the measured pressure ratio at the geometric throat is much greater than the expected isentropic value of 0.544, for an isentropic exponent of $k = 1.3$, showing that the effective throat is actually downstream of the geometric throat.

2) As the stagnation temperature is sufficiently lowered below the value corresponding to the lowest curve, the measured p/p_o at some point in the nozzle becomes higher than the corresponding p/p_o in the reference curve. Downstream of this point, measured p/p_o are everywhere higher than in the reference curve. This deviation of measured pressure ratios from the reference values is taken as a sign of condensation from the vapor. The condensed fluid releases its enthalpy of vaporization to the remaining gaseous phase, which results in a change in stagnation temperature of the fluid. From one-dimensional

considerations and for effect of heat addition alone, it is known that

$$\frac{dP}{P} = -\frac{kM^2}{1-M^2}\left(\frac{dQ}{C_pT}\right) \tag{19}$$

Hence, in supersonic flow, such a heat release to the vapor may be

expected to lead to a pressure rise as shown by the data.

3) As the temperature is further lowered, the point of pressure

deviation moves upstream, and the deviations from the non-condensing

curve at any cross-section becomes greater, as seen from equation (19),

when M $\rightarrow$ 1 from values $>$ 1.

4) With further decrease in stagnation temperature the pressure

curve actually begins to exhibit a definite minimum and maximum, and

the location of this minimum is in general different from the point of

deviation of the curve from the non-condensing curve. We have used

the convention that if the distribution does not show a definite min-

imum and maximum, then the onset of condensation is defined as the point

of departure from the non-condensing curve. Otherwise, the minimum

point of the curve is chosen.

It has been observed that the non-condensing curves are themselves

dependent on the pressure level. This effect is illustrated in Figure 16.

At the lowest stagnation pressure the non-condensing curve follows the path

A - C. With increasing stagnation pressures, however, it begins to approach

the path B downstream of the nozzle, while still keeping very close to path

A upstream, until, at about 60 psi stagnation pressure, it actually does

follow the path A - B. This justifies the statement made earlier that

frictional effects are mostly confined to the section of the nozzle down-

stream of the throat. It was further observed, however, that with pressures

between 60 - 70 psi (Figures 14 & 15) the non-condensing curve shows a

shift to path D in the upstream side of the nozzle, and follows path D - B.

It is believed that this further shift is not due to friction for, although

we have seen that frictional effects are much greater in the supersonic than in the subsonic region, there is hardly any noticeable shift in the supersonic section within the same interval of pressure increase as the subsonic path shifts from A to D. Furthermore, the flow along path D was observed to be very unsteady, particularly within a small distance of the geometric throat. This may be seen from Figure 18. As this observation seems to be independent of the initial superheat of the vapor, it cannot possibly be due to condensation occurring too near the throat, as we had thought earlier. The unsteadiness is in fact greater for the higher superheats. It is postulated that these disturbances could have been caused by non-uniformities in the entering flow which, while unnoticeable at lower pressures, became magnified as the pressure increased.

Figure 17 shows pressure distributions obtained from the two-dimensional nozzle with a total included angle of 3°. They illustrate the same qualitative features as those earlier described. The initial superheats and degree of supersaturation achieved just before condensation are shown on the charts. Contrary to the findings of Duff[21] it does not seem that there is any definite correlation between the initial superheat and final degree of supersaturation attained, although at the higher pressures used in our experiments, the supersaturation tended to increase as the shock moves towards the throat, but even this is contrary to Duff's results. In this respect, our present findings are in agreement with the experiments of Binnie and Woods[9] on steam.

It may be asked at this point what effect the wall has on the condensation? A rough heat transfer analysis showed that the nozzle wall is superheated relative to the free stream pressure and, hence, cannot possibly initiate the condensation process, which may thus be regarded as essentially a free-stream phenomenon.

III. NUMERICAL CALCULATIONS

A. Isentropic Expansion

Before condensation occurs, the flow through the nozzle is considered to be:

one-dimensional, steady, isentropic.

The stagnation conditions in the stagnation tank before the entrance of the nozzle are:

$$p = p_0, \quad T = T_0, \quad V = V_0 = 0.$$

The cross-sectional area at any place x, A = f(x), is given by the geometric design of the nozzle. From this A = f(x), the unknown properties p, T, V = f(A) or f(x) at any point x along the nozzle, can be calculated from the equations for choking flow, (see Ref. (22):

$$\left. \begin{aligned} \frac{A}{A^*} &= \frac{1}{M} \left[\frac{2 + (K-1)M^2}{K+1} \right]^{\frac{K+1}{2K-2}} \\ \frac{p}{p_0} &= \left[1 + \frac{K-1}{2} M^2 \right]^{-\frac{K}{K-1}} \\ \frac{T}{T_0} &= \left[1 + \frac{K-1}{2} M^2 \right]^{-1} \end{aligned} \right\} \quad (20)$$

With the Mach number M herefrom known, the velocity V is given by:

$$V = M \cdot \sqrt{k \, g \, R \, T} = M \cdot a, \quad \text{where } a = \sqrt{k \, g \, R \, T}$$

is the local velocity of sound in the vapor.

The mass flow for choking flow at the throat is given by:

$$\dot{m} = A^* \psi_{max} \, p_0 \cdot \sqrt{\frac{2g}{R \, T_0}}$$

where $\quad \psi_{max} = \left(\frac{2}{K+1} \right)^{\frac{1}{K-1}} \cdot \sqrt{\frac{K}{K+1}}$

where $k = c_p/c_v$ is the isentropic exponent at the conditions at the throat.

B. Nucleation Rate I

The expansion is considered to remain isentropic until the nucleation rate I = f(p, T) reaches a characteristic critical value I_{cr} which we chose to be 10^{10} nuclei/ft³ sec). The onset of condensation was found to be relatively independent of the assumed value of I_{cr} when I_{cr} was varied between the limits from 1 to 10^{20} nuclei/ft³ sec). As soon as I = f(p, T) $\geq I_{cr}$, the

isentropic calculation is finished and condensation effects are taken into the further calculation procedure.

The expression for the nucleation rate I is:

$$I = \left(\frac{p}{kT}\right)^2 \cdot v \cdot \sqrt{\frac{2}{\pi}\frac{\sigma}{m}} \cdot e^{-\left[\frac{4\pi \sigma (r^*)^2}{3kT}\right]} \tag{21}$$

where

$$r^* = \frac{2\sigma}{\rho_L \cdot RT \cdot \ln(P/P_{S\infty})} \tag{22}$$

is the critical drop radius from equation (6). Drops greater than r* can grow, drops smaller than r* vaporize again. The surface tension σ is, since the droplets are very small, assumed to be considerably different from the flat film surface tension σ_∞. A brief discussion about necessary corrections to the surface tension follows in Part IV, B. Here the assumption according to Tolman[26] is used:

$$\sigma = \frac{\sigma_\infty}{1 + \delta/r^*} \tag{23}$$

where δ is a length between 0.50 and 1.20 of the molecular radius r_M.

The surface tension of the flat film surface σ_∞ is dependent on the temperature T, see Ref. (24):

$$\sigma_\infty = \frac{K_E \left(T_K' - T\right)}{\left(\frac{\bar{A}}{\rho_L}\right)^{2/3}} \tag{24}$$

where
K_E = Eötvös constant

$T_K' \approx T_K$ = critical temperature

$\bar{A}$ = molecular weight

ρ_L = liquid density

Now the quantity y, is defined so that $r^* = \sigma/y$, where

$$y = 0.5 \, \rho_L \cdot RT \cdot \ln\left(\frac{p}{P_{S\infty}}\right);$$

then the surface tension becomes

$$\sigma = \sigma_\infty - \delta \cdot y = \sigma_\infty - \frac{\delta}{r_M} \cdot r_M \cdot y$$

Substitution of σ and y into equation (21) gives:

$$I = \left(\frac{P_{S\infty}}{kT}\right)^2 \left(\frac{p}{P_{S\infty}}\right)^2 \cdot v \cdot \sqrt{\frac{2}{\pi}\frac{\sigma}{m}} \cdot \sqrt{\sigma} \cdot e^{-\left[\frac{4\pi}{3kT} \cdot \frac{\sigma^3}{y^2}\right]} \tag{25}$$

The molecular mass m and the molecular volume v are:

$$m = \frac{\bar{A}}{N_0} \quad ; \quad v = \frac{m}{\rho_L} = \frac{4}{3}\pi \cdot r_M^3$$

where the molecule is assumed to be a sphere of radius r_M:

$$r_M = \sqrt[3]{\frac{3}{4\pi}} \cdot \sqrt[3]{v} = 0.620351 \cdot \sqrt[3]{v}$$

Figure 19 shows lines of constant nucleation rate in a p, t-diagram, obtained from equation (25). It illustrates how rapidly the nucleation rate increases during the expansion after saturation is reached. A few isentropic expansion lines are drawn to show this.

C. Calculation of Pressure, Temperature and Velocity along the Nozzle under Consideration of the Presence of Liquid Parts

The following further assumptions are made:

a) one-dimensional, steady flow

b) no heat transfer from the surrounding walls

c) no friction at the walls

For the flow in the nozzle the basic equations are written for a control volume of the length dx:

a) Continuity Equation

$$\frac{V \cdot A \cdot \rho}{(1-\mu)} = \dot{m} = const \tag{26a}$$

or

$$\frac{1}{V}\frac{dV}{dx} + \frac{1}{\rho}\frac{d\rho}{dx} + \frac{1}{(1-\mu)}\frac{d\mu}{dx} = -\frac{1}{A}\frac{dA}{dx} \tag{26b}$$

b) Momentum Equation

$$-A\,dp - A\rho V\,dV = 0 \tag{27a}$$

or

$$\frac{1}{V}\frac{dV}{dx} + \frac{1}{V^2}\cdot\frac{1}{\rho}\cdot\frac{dp}{dx} = 0 \tag{27b}$$

c) Energy Equation

$$(1-\mu)\,dh_g + \mu \cdot dh_L - d(\mu \cdot h_{fg}) + V\,dV = 0 \tag{28a}$$

or

$$(1-\mu)\frac{dh_g}{dx} + \mu\frac{dh_L}{dx} - \frac{d(\mu \cdot h_{fg})}{dx} + V\frac{dV}{dx} = 0 \tag{28b}$$

d) Equation of State of a Perfect Gas

$$p = \rho R T \tag{29}$$

By definition:

$$M = \frac{V}{\sqrt{kg\,RT}} \qquad \text{and } K = \frac{C_p}{C_v}$$

We introduce a dimensionless parameter

$$\lambda = \frac{h_{fg}}{c_p \cdot T}$$

After replacing ρ by p and T and introducing the Mach number M the equations (26), (27) and (28) become:

Continuity:
$$\frac{1}{V}\frac{dV}{dx} + \frac{1}{P}\frac{dp}{dx} - \frac{1}{T}\frac{dT}{dx} = -\frac{1}{A}\frac{dA}{dx} - \frac{1}{(1-\mu)}\frac{d\mu}{dx}$$

Momentum:
$$K\cdot M^2 \cdot \frac{1}{V}\frac{dV}{dx} + \frac{1}{P}\frac{dp}{dx} = 0 \tag{30}$$

Energy:
$$\frac{1}{T}\frac{dT}{dx} + (K-1)M^2 \cdot \frac{1}{V}\frac{dV}{dx} = \frac{1}{c_p T} \cdot \frac{d(\mu \cdot h_{fg})}{dx}$$

Remark: An intermediate step in the energy equation gives:

$$\frac{c_{pg}\cdot dT_g}{dx} - \mu\left[\frac{c_{pg}\,dT_g - c_{pL}\,dT_L}{dx}\right] - \frac{d(\mu \cdot h_{fg})}{dx} + V\frac{dV}{dx} = 0$$

where the second term is neglected because of the small amount of μ.

From these the three unknown properties p, T, V can be estimated:

$$\frac{dp}{dx} = p\cdot\frac{KM^2}{M^2-1}\left[\left(\lambda - \frac{1}{(1-\mu)}\cdot\frac{d\mu}{dx} - \frac{1}{A}\frac{dA}{dx}\right]\right.$$
$$\frac{dV}{dx} = -\frac{V}{KM^2}\cdot\frac{1}{P}\frac{dp}{dx} \tag{31}$$
$$\frac{dT}{dx} = T\cdot\frac{K-1}{K}\cdot\frac{1}{P}\frac{dp}{dx} + \lambda\,\frac{d\mu}{dx}\cdot T$$

In order to find the distribution p, V, T = f(x) the derivative $d\mu/dx$ has to be determined. (A and dA/dx are known from the geometry of the nozzle).

D. The Liquid Part μ and Its Derivatives

The liquid-mixture mass ratio μ is given at any instantaneous point x along the nozzle by the following considerations:

1) small droplets (nuclei) of radius r_o have been built on a nucleation rate I = f(p, T) in the past length along the nozzle. ($0 \rightarrow \xi \rightarrow x$).
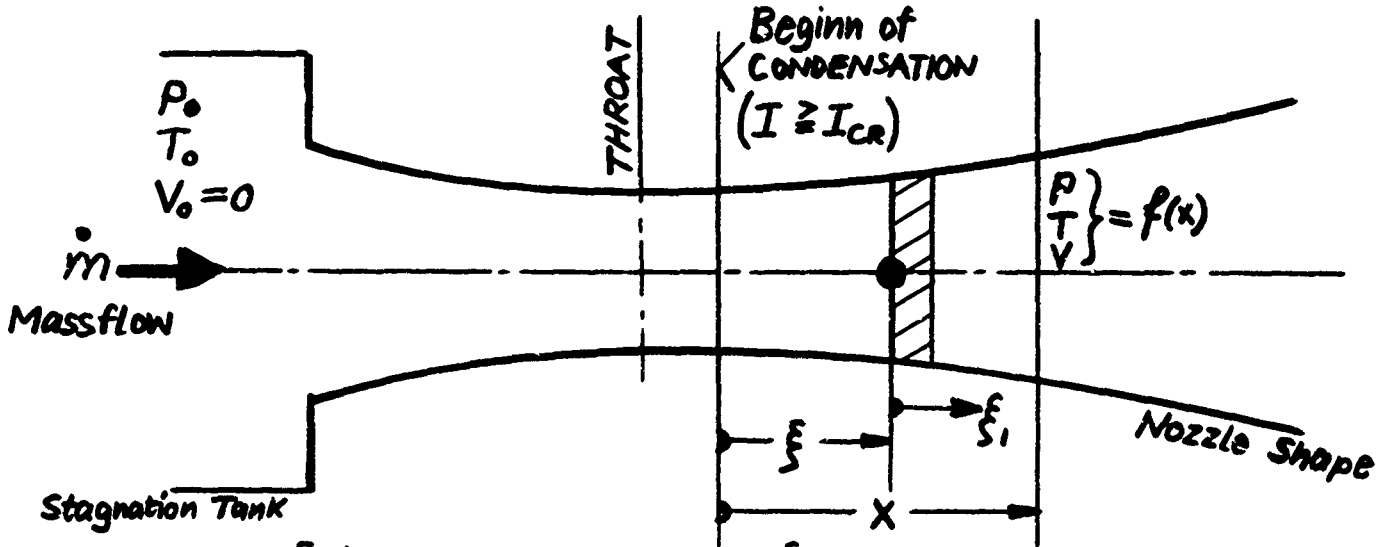
2) those nuclei grew, and their radius r increased by $\partial r/\partial x =$ f(p, T) steadily from the point where they were built ξ_1 to the point x($\xi_1 \rightarrow \xi \rightarrow x$).

It is assumed, that at any point x <u>all</u> the droplets grow at the same rate:
$\partial r / \partial x \approx dr/dx$, regardless of their size.

The experession for μ at the point x is given by the following expression, where ξ and ξ_1 are dummy variables, as shown in the sketch:

$$M(x) = \frac{1}{\dot{m}} \int_{\xi=0}^{\xi=x} \rho_L \cdot I \cdot A(\xi) d\xi \frac{4\pi}{3} \left(r_0(\xi) + \int_{\xi_1=\xi}^{\xi_1=x} \frac{dr}{d\xi_1} d\xi_1 \right)^3 \tag{32}$$

Application of Leibniz' rule gives:

$$\frac{d\mu}{dx} = \frac{\rho_L}{\dot{m}} S \frac{dr}{dx} + \frac{\rho_L}{\dot{m}} I A(x) \cdot \frac{4\pi}{3} r_0^3(x) \tag{33a}$$

where $S = \int_{\xi=0}^{\xi=x} I A(\xi) d\xi \cdot 4\pi \cdot r(\xi,x)^2$ $\tag{33b}$

Repetitive application gives:

$$\frac{dS}{dx} = Z \cdot \frac{dr}{dx} + I A(x) \cdot 4\pi \, r_0(x)^2 \tag{34}$$

where $Z = \int_{\xi=0}^{\xi=x} I A(\xi) d\xi \cdot 8\pi \cdot r(\xi,x)$

and $\frac{dZ}{dx} = ZI \frac{dr}{dx} + I A(x) \cdot 8\pi \cdot r_0(x)$ $\tag{35}$

where $ZI = \int_{\xi=0}^{\xi=x} I A(\xi) d\xi \cdot 8\pi$

and $\frac{dZI}{dx} = I A(x) \cdot 8\pi$ $\tag{36}$

After this we have the following system of necessary equations:

$$\frac{dZl}{dx} = I \cdot A(x) \cdot 8\pi$$

$$\frac{dZ}{dx} = Zl \cdot \frac{dr}{dx} + I \cdot A(x) \cdot 8\pi \cdot r_0(x)$$

$$\frac{dS}{dx} = Z \cdot \frac{dr}{dx} + I A(x) \cdot 4\pi \cdot r_0^2(x)$$

$$\frac{d\mu}{dx} = \frac{\rho_L}{\dot{m}} S \frac{dr}{dx} + \frac{\rho_L}{\dot{m}} I \cdot A(x) \cdot \frac{4\pi}{3} \cdot r_0^3(x)$$

$$\frac{dp}{dx} = p \cdot \frac{\kappa M^2}{M^2 - 1} \cdot \left[\left(\lambda - \frac{1}{(1-\mu)} \right) \frac{d\mu}{dx} - \frac{1}{A}\frac{dA}{dx} \right]$$

$$\frac{dV}{dx} = -\frac{V}{\kappa M^2} \cdot \frac{1}{p} \frac{dp}{dx}$$

$$\frac{dT}{dx} = T \cdot \frac{\kappa-1}{\kappa} \cdot \frac{1}{p} \frac{dp}{dx} + \lambda \frac{d\mu}{dx} \cdot T$$

$$\left. \right\} \quad (37)$$

E. The Size of the Droplets r_0 and Their Growing Rate dr/dx

According to Ref. (13) the radius of the newly built droplets r_0 is about 1.3 times the critical radius r*:

$$r_0 \approx 1.3 \, r^* = \frac{2.6 \cdot \sigma}{\rho_L \cdot RT \cdot \ln(P/P_{s\infty})}$$

The growing rate of the drop radius dr/dx is obtained from the equations (13) and (14):

$$\frac{dr}{dx} = \frac{3p}{2V \cdot u_{fg} \cdot \rho_L \cdot \sqrt{2\pi RT}} \cdot \left[RT_D - RT \right] \qquad (38)$$

where the drop temperature T_D is given by equation (15):

$$\frac{2}{3}\frac{u_{fg}}{RT} \cdot \xi \left[1 - \frac{P_{s\infty,DROP}}{P} \cdot e^{\left(\frac{2\sigma}{\rho_L \cdot R \cdot T_D \cdot \widehat{r}} \right)} \cdot \sqrt{\frac{T}{T_0}} \right] = \frac{T_D}{T} - 1 \quad (15)$$

In this expression the drop radius $\widehat{r}$ is unknown. Here it is assumed that $\widehat{r}$ is an average drop radius of all the drops which strike the cross-section area A at the point x. The total surface S of all these drops passing the area A at the point x per second is given by equation (33b):

$$S = 4\pi \, \widehat{r}^2 \int_0^x I A(\xi) \, d\xi$$

and the total mass of all those droplets is given by equation (32):

$$\mu \cdot \dot{m} = \rho_L \cdot \frac{4}{3}\pi \cdot \widehat{r}^3 \int_0^x I A(\xi) \, d\xi$$

So the average drop radius becomes

$$\widehat{r} = \frac{3 \dot{m} \cdot \mu}{\rho_L \cdot S}$$

The drop temperature T_D has to be computed from equation (15). Since $p_{S\infty,drop}$ herein is the saturation pressure corresponding to T_D, and all the properties u_{fg}, σ, ρ_L are functions of T_D, it is complicated to solve analytically for T_D. (Besides this, the surface tension σ depends on the average drop radius $\bar{r}$ too.) Therefore, equation (15) is solved iteratively starting with a first guess $T_D = T$.

F. Numerical Solution of the Differential Equations (37)

Equation (37) is a system of seven simultaneous first order differential equations. They are solved step-wise by a fourth order Runge-Kutta method, which is ready to use and written up as the Subroutine #1381 "RUNGE" of the M. I. T. Computation Center. This program adjusts the initially given step-size according to the demanded permissible relative errors, which we took as 0.00001. The starting values are given at the point $x_{(o)}$, where the nucleation rate $I \geqq I_{cr}$ is reached. There, the starting values;

$$zl_{(o)} = 0; \quad z_{(o)} = 0; \quad S_{(o)} = 0; \quad \mu_{(o)} = 0; \quad \text{and} \quad p_{(o)}, V_{(o)}, T_{(o)}$$

are the properties which are calculated by the isentropic expansion.

Remarks: The physical and thermodynamic properties for Ammonia were taken from the following references:

> Surface tension   :   References (24) and (25)
>
> Saturation pressure $p_{S\infty}$
> Liquid density ρ_L
> Specific heat c_p
> Vaporization heat h_{fg} $\Big\}$ Reference (23)

IV. VARIATION OF THE CALCULATION PROGRAM

A. Correction for Frictional Effects

Because of the discrepancy between the non-condensing curve and the isentropic line, based on the geometry of the nozzle, an effective nozzle profile has been selected based on the measured pressure distribution:

The relation between the measured p/p_o and the effective A/A^* is given by:

$$\frac{p}{p_o} = \left[1 + \frac{K-1}{2} M^2 \right]^{-\frac{K}{K-1}}$$

$$\frac{A}{A^*} = \frac{1}{M} \left[\frac{2 + (K-1)M^2}{K+1} \right]^{\frac{K+1}{2K-2}}$$

Figure 20 shows a comparison between the isentropic pressure distribution for the geometrical nozzle profile, and that corresponding to the effective nozzle geometry.

B. Uncertainties in the Physical Properties Entering the Nucleation and Drop·Growth Theory

a) Surface Tension σ :

The correction to the flat film surface tension, used in the calculation procedure, was given in equation (23):

$$\sigma = \frac{\sigma_\infty}{1 + (\sigma/r_M) \cdot (r_M/r^*)} \tag{23}$$

Herein the correction factor σ/r_M according to Tolman[26] is recommended to lie between 0.50 and 1.20. Figure 21a shows the effect of the surface tension on the pressure distribution.

b) The Factor ξ in the Drop Growing Equations:

The factor ξ was defined as the number of condensed particles to the total number of arriving particles striking the drop surface area.

Calculations were done with constant values for σ/r_M for different values of ξ : ξ was modified to be 0.04, 0.20, 0.50 and 0.80. It turned out that the p/p_o-values for a given x did not change by more than 1.5 per cent in this range of ξ ; therefore the conclusion that the factor ξ is quite insignificant to the results is obvious. For the further calculations $\underline{\xi = 0.50}$ was used always.

c) A Complete Change in the Nucleation Rate

Following the suggestion of Lothe and Pound[28] the nucleation rate, I, as calculated in the described manner, according to equation (25), was multiplied by a factor of 10^{17}:

$$I \rightarrow 10^{17} \cdot I_{eq.(25)}$$

Thereby no correction for the surface tension was made: $\delta/r_M = 0$

The results of this change in the nucleation rate are shown in Figures 21b and 22.

V. COMPARISON OF EXPERIMENTS AND THEORY

Figure 20 shows the non-condensing line and the experimentally measured pressure distribution for the stagnation conditions $p_o = 50.5$ psia; $t_o = 58°F$. In the same graph the theoretical isentropic line, based on the geometric design of the nozzle is shown. The theoretical pressure distributions for both the effective areas from the experimental non-condensing line and for the geometric areas are shown. One notices that the pressure values for the two different areas are considerably different, and since the method of using the effective areas from the measured non-condensing line approaches the experimental results in the order of magnitude much better, this method is further used for all calculations; especially the difference in the location of the throat is evident. The theoretical calculations in Fig. 20 are done with $\delta/r_M = 0.80$ and $\xi = 0.50$, with no other correction to the nucleation rate, I, as given in equation (25). It is seen that the theory shows a considerable delay in condensation as compared to the experiment, a delay which might have to do with uncertainties in the surface tension.

Figure 21a shows how the quite uncertain correction term for the surface tension δ/r_M affects the theoretical pressure distribution. Based on the areas computed from the non-condensing line for $p_o \approx 45$ psia, pressure distributions for the following stagnation conditions are shown:

$$p_o = 46.9 \text{ psia}; \quad t_o = 40°F$$
$$47.0 \text{ psia} \qquad 54°F$$
$$44.8 \text{ psia} \qquad 67°F$$

For these stagnation conditions the theoretical curves with $\delta/r_M =$ 0.50, 0.80 and 1.20 are drawn.

The result of this set of curves shows that an increase of δ/r_M, which means a decrease in the surface tension σ, moves the onset of condensation towards the upstream direction of the nozzle. For the case of $p_o = 46.9$ psia, $t_o = 40°F$ the value of $\delta/r_M = 1.20$ would predict condensation somewhat upstream of the throat in the subsonic part of the nozzle, and for this case the theoretical calculation cannot be performed since the mass flow computation is based on choking flow of the uncondensed vapor. The experimental pressure distributions are plotted into the same figure. It appears that the higher values of $\delta/r_M = 0.80$ or 1.20 agree better with the experiments, showing that a possible way to improve the theory would consist in studying more closely the influence of the small size of the drops on their surface tension.

Figure 21b shows the effect of multiplying the nucleation rate by a factor of 10^{17}. It is seen that this also brings the theoretical pressure distribution into better agreement with the experimental distribution.

In Figure 22 the pressure and temperature values for the onset points of the condensation are shown. Here, the onset of condensation is supposed to be the point in the pressure distribution curve along the nozzle, where $dp/dx = 0$ in case of an observed minimum point, (see case A in the sketch) or where $d^2p/dx^2 = 0$ in case one cannot find a definite minimum point, (see case B in the sketch).

The theoretically computed pressure distribution curves always show a definite minimum pressure point, and the locations of the theoretically predicted points of condensation onset are drawn as continuous lines in the

graph. Three theoretical curves have been shown, two for $\delta/r_M = 0$ and $\delta/r_M = 0.80$, with no other correction to I, and one in which I has been multiplied by 10^{17}, with no correction for δ.
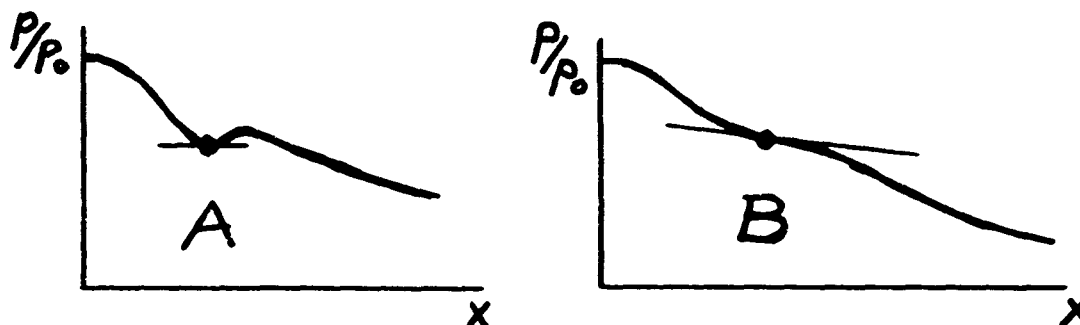
VI. CONCLUSION

From the foregoing the following conclusions may be made:

1) Ammonia shows less supersaturation than is predicted by the Becker-Doring (Frenkel-Zeldovich) Nucleation Rate Equation, the degree of supersaturation observed in all the tests lying between 1.5 and 2.5.

2) Corrections to the surface tension may be a very important part of the nucleation theory, which therefore ought to be given greater consideration than heretofore.

3) The closer agreement obtained between theory and experiment when the nucleation rate equation is multiplied by 10^{17} lends some support to the gassification concept, proposed by Lothe and Pound[28], and by Oriani and Sundquist[30], although it remains doubtful how much of this correction factor is due to uncertainties in surface tension, and how much is due to gassification.

4) A lot of scatter is evident on the curve in which an attempt has been made to plot a condensation line. This is mostly due to uncertainties in the exact shape of the pressure discontinuity, as may be seen from the curves.

5) There does not seem to be any definite correlation between the initial superheat and final degree of supersaturation attained before condensation occurs, which may be partly due to the scatter in the results,

but in the higher pressures used in the experiments, the supersaturation
tended to increase as the pressure discontinuity moves upstream. This
finding is contrary to that of Duff[21] although in agreement with those of
Binnie and Woods[9].

VII. SUGGESTIONS FOR FURTHER WORK

Since for the case of a turbine nozzle, the most interesting property
is the exit velocity at the exit area of the nozzle, a measured velocity
distribution along the nozzle would be very useful. Due to the fact that
condensation occurs only in the supersonic part of the nozzle velocity
measurements are quite difficult for the very small dimensions of the
nozzle.

Temperature measurements could be done either by optical methods or
by using thermo-couples, but even for this problem the dimensions of the
nozzles used are too small.

For further work to study velocity, temperature and pressure distrib-
utions which differ from the simplified one-dimensional case a much bigger
nozzle is recommended and this would require a closed cycle with a condenser
after the nozzle, followed by a compressor. In this case the minimal tem-
perature at the low pressure side would give trouble in the condenser.
Therefore, the whole cycle would probably demand a higher pressure level.

It might be possible to reduce the scatter by obtaining a more exact
shape of the pressure distribution, especially near the discontinuity.
This could be done by using a search tube instead of pressure taps, so
that the pressure points could be made as closely spaced as possible.

Perhaps direct measurements of actual size of condensed droplets, by
light scattering or other techniques, could lead to a better understanding
of the phenomenon of drop growth, and to a better appraisal of the theory.

In any case, a better temperature control than the one adopted in these experiments would be a desirable improvement.

REFERENCES

1. Wilson, C. T. R. - Phil. Trans. Royal Soc., Vol. A192, p. 403 (1899) - also - Phil. Trans. Royal Soc., Vol. A193, p. 289 (1899).

2. Powell, C. F. - Proc. Royal Soc. (London), Vol. A119, p. 553 (1928).

3. Volmer, M. and H. Flood - Z. Physik Chemie, Vol. A170, p. 273 (1934).

4. Hill, P. G. - "Homogeneous Nucleation of Supersaturated Water Vapor in Nozzles" - Gas Turbine Laboratory Report #78 - M. I. T. - Jan. 1965.

5. Stodola, A. - Steam and Gas Turbines - McGraw-Hill Book Co., Inc. (1927) pp. 117 - 128, 1034 - 1073.

6. Yellot, J. I. - Trans. ASME, Vol. 56, p. 411 (1934).

7. Yellot, J. I. and C. K. Holland - Trans. ASME, Vol. 59, p. 171 (1937).

8. Rettaliata, J. T. - Trans. ASME, Vol. 58, p. 599 (1936).

9. Binnie, A. M. and M. W. Woods - "The Pressure Distribution in a Convergent-Divergent Steam Nozzle" - Proc. Inst. Mech. E., Vol. 138, pp. 229 - 266 (1936).

10. Oswatitsch, K. and Z. Angew - Math. u. Mech, Vol. 22, pp. 1 - 13 (1942).

11. Hill, P. G., H. Witting, and E. P. Demetri - "Condensation of Metal Vapors During Rapid Expansion" - Trans. ASME, Vol. 62 - WA-123 (1963).

12. Volmer, M. - Kinetic der Phasenbilding - Steinkopf, Dresden u. Leipzig (1939), Chapter 4.

13. Becker, R. and W. Doering - Ann. der Phys., Vol. 24, p. 719 (1935).

14. Zeldovich, J. J. - Exp. Theor. Phys. (Russ.), Vol. 12, p. 525 (1942).

15. Frenkel, J. - Kinetic Theory of Liquids - Oxford Univ. Press (1946), Chapter 7.

16. Wegener, P. P. and A. A. Pouring - "Experiments on Condensation of Water Vapor by Homogeneous Nucleation in Nozzles" - J. Phys. of Fluids, Vol. 1, p.p. 352 - 361 (1964)

17. Wegener, P. P. and L. M. Mark - "Condensation in Supersonic and Hypersonic Wind Tunnels" - Adv. in Appl. Mech., Vol. V, (1958).

18. Launder, B. E. -"An Improved Pohlhausen-Type Method of Calculating the Two-Dimensional Laminar Boundary Layer in a Pressure Gradient" - ASME 63-HT-26 (1963).

19. Courtney, W. G. - J. Chem. Phys., Vol. 36, p. 2018 (1962).

20. Matheson Gas Data Book - Matheson Company Inc. - James Grey, Inc. (1961).

21. Duff, K. M. - "Condensation of CO_2 in Supersonic Nozzles" - Gas Turbine Laboratory Report No. 76 - M. I. T. - (1964).

22. Shapiro, A. H. - <u>The Dynamics and Thermodynamics of Compressible Fluid Flow</u> - Vol. I - The Ronald Press Co. - New York.

23. <u>Handbuch der Kältetechnik</u> - Vol. 4 - Springer-Verlag - Berlin/Göttingen/Heidelberg - (1956).

24. Landolt-Börnstein · <u>Zahlenwerte und Funktionen</u> - Vol. II, Part 3 - Springer-Verlag - Berlin/Göttingen/Heidelberg - (1956)

25. <u>Handbook of Chemistry and Physics</u> - 43rd. Edition - The Chemical Publishing Co. - Cleveland, Ohio - (1961-62).

26. Tolman, R. C. - Jour. Chem. & Physics - Vol. 17, pp. 333-337 - (1949).

27. Hirn, G. A. & Cazin - "Comptes Rendus de l'Academie Francaise" - Vol. 63, p. 1144 - (1866).

28. Lothe, J. & Pound, G. M. - "Reconsiderations of Nucleation Theory" - Jour. Chem. & Physics - Vol. 36, pp. 2080-2085 - (1962).

29. Courtney, W. G. - Jour. Chem. & Physics - Vol. 36, p. 2009 - (1962).

30. Oriani, R. A. & Sundquist, B. E. - "Emendations to Nucleation Theory and the Homogeneous Nucleation of Water from the Vapor" - Jour. Chem. & Physics - Vol. 38, pp. 2082-2089 - (1963).

APPENDIX: Computer Program in FORTRAN

```
C       )RTRAN PROGRAM FOR EXPANSION OF AMMONIA IN NOZZLES


C       MAIN PROGRAM
C       READ DATA
        READ 1,ANO,BOLK,G
      1 FORMAT (2E14.6,F10.0)
        READ2,A,TK,EOT
      2 FORMAT (3F10.0)
        READ4,DELX,DELMA
      4 FORMAT(2F10.0)
        READ5, DELM,DELTAU
      5 FORMAT (2F10.0)
        READ6, DELR,XI
      6 FORMAT (2F10.0)
        READ 667,AJKR
        READ 667,FACTOR
    667 FORMAT (E14.6)
        READ 67,ASTAR,XSTAR
     67 FORMAT (2F10.0)
        READ 7,M
      7 FORMAT (I10)
        DO 777 I=1,M
    777 READ 77,XT(I),PADT(I)
     77 FORMAT (2F10.0)
        READ 7001,TOL(1),TOL(2),TOL(3),TOL(4),TOL(5),TOL(6),TOL(7)
   7001 FORMAT (7F10.0)
       OREAD 7002,YMIN(1),YMIN(2),YMIN(3),YMIN(4),YMIN(5),YMIN(6),YMIN(7)
   7002 FORMAT (7F10.0)
        READ 7003,L,DXOUT
   7003 FORMAT (I10,F?0.0)
        READ 7004,MARK(2)
   7004 FORMAT (I10)
        READ 8,BETA
      8 FORMAT (F10.0)
     33 READ3,PZERO,TZERO
      3 FORMAT (2F10.0)
        READ 81,NUMBER
     81 FORMAT (I1)
C       PART 1
        PRINT 298,PZERO
    298 FORMAT (10H  PZERO = E20.8)
        PRINT 299,TZERO
    299 FORMAT (10H  TZERO = E20.8)
        PRINT 300
   3000FORMAT(110H          X                    AC                     M
       1                P              V                T ///)
        COMMON BETA,M,I,XT,RADT
        COMMON TK,EOT,A,R,ANO,BOLK,G,DELR,XI,DELTAU,AMASS     ,FACTOR
        DIMENSION I(50),XT(50),RADT(50)
        R=ANO*BOLK/A
        T=TZERO
        X=0.0
     10 X=X+DELX
```

```
      CALL NOZZLE(X,AC,DADX)
      CP=0.4212+0.0151*T/100.+0.0038051*(T/100.)*(T/100.)
      CP=42700.*CP
      AK=CP/(CP-R)
      A1=(AK-1.)/(AK+1.)
      A2=(AC/ASTAR)**(2.*A1)
      IF (X-XSTAR) 15,16,17
   16 AMACH=1.0
      GO TO25
   15 AMACH=0.0
  200 YMACH=A2*AMACH**(2.*A1)-A1*AMACH**2 -2./(AK+1.)
      IF (YMACH) 56,25,58
   56 XA=AMACH
      AMACH=AMACH+DELMA
      GO TO 200
   58 XB=AMACH
      AMACH=0.5*(XA+XB)
      GO TO 20
   17 AMACH=1.0
 2000 YMACH=A2*AMACH**(2.*A1)-A1*AMACH**2 -2./(AK+1.)
      IF (YMACH) 158,25,156
  156 XA=AMACH
      AMACH=AMACH+DELMA
      GO TO 2000
  158 XB=AMACH
      AMACH=0.5*(XA+XB)
   20 YMACH=A2*AMACH**(2.*A1)-A1*AMACH**2 -2./(AK+1.)
      DYMACH=2.*A1*(A2*AMACH**((AK-3.)/(AK+1.))-AMACH)
      AMAC=AMACH-YMACH/DYMACH
      IF(ABSF(AMAC-AMACH)-DELM) 21,21,22
   22 AMACH=AMAC
      GO TO20
   21 AMACH=AMAC
   25 DENOM=1.+0.5*(AK-1.)*AMACH**2
      T=TZERO/DENOM
      P=PZERO/DENOM**(AK/(AK-1.))
      V=AMACH*SQRTF(AK*G*R*T)
      PRINT 69,X,AC,AMACH,P,V,T
   69 FORMAT (6E20.8)
    0 PLG=9.584586-1648.6068/T-1.638646*T*0.01
    1 +2.403267*T*T*0.00001-1.168708*T*T*T*0.00000001
      PSIN=EXPF(2.302585*PLG)
      PSIN=1000.*PSIN
      IF (P-PSIN) 10,10,205
C         PART 2
  205     RHO = 235. + 0.654*(TK-T) + 62.77*(TK-T)**0.333333
          RHOG = 235. + 0.654*(TK-T) - 62.77*(TK-T)**0.333333
          RHO = 0.001*RHO
          RHOG = 0.001*RHOG
          SIGIN = EOT*(TK-T)/(A/RHO)**0.666667
          HFG = 32.938*SQRTF(406.16 - T) - 0.5890*(406.16 - T)
          HFG = 42700.*HFG
          UFG = HFG - PSIN*(1./RHOG - 1./RHO)
          CP = 0.4212 + 0.0151*T/100. + 0.0038051*T*T/10000.
          CP = CP*42700.
```

```
      AK = CP/(CP-R)
      AM = A/ANO
      AV = AM/RHO
      RM = 0.620351*AV**0.333333
      C1 = 0.797885*(PSIN/T)**2 *AV/BOLK *SQRTF(G/AM)/BOLK
      C2 = 4.18879/(BOLK*T)
      AY = 0.5*RHO*R*T*LOGF(P/PSIN)
      SIG = SIGIN - DELR*RM*AY
      AJ = C1*(P/PSIN)**2 * SQRTF(SIG)*EXPF(-C2*SIG**3/AY**2)
      AJ=AJ*FACTOR
      IF (AJ - AJKR)  100, 100, 400
100   GO TO 10
400   N = 7
      PRINT 310
  310 FORMAT(22H  CONDENSATION  OCCURS)
      PRINT 311,AJ
  311 FORMAT(7H  AJ+  E20.8)
      PRINT 320
 3200FORMAT(102H               X              Z1              Z              S
     1          MU              P              V              T/)
C     AMASS-COMPUTATION
      PSIMAX=(2./(AK+1.))**(1./(AK-1.))*SQRTF(AK/(AK+1.))
      AMASS=ASTAR*PSIMAX*PZERO*SQRTF(2.*G/(R*TZERO))
      Y(1) = 0.0
      Y(2) = 0.0
      Y(3) = 0.0
      Y(4) = 0.0
      Y(5) = P
      Y(6) = V
      Y(7) = T
      H = DELX
      XOUT(1) = X
      DO 401 K=2,L
  401 XOUT(K) = XOUT(K - 1) + DXOUT
      MARK(1) = 1
      MARK(3) = 3
      MARK(4) = 0
      MARK(5) = 1
      DIMENSION  Y(7), YMIN(7), TOL(7), XOUT(200), MARK(5)
      CALL RUNGE(N, X, Y, TOL, YMIN, H, XOUT, MARK)
      GO TO (33,30),NUMBER
   30 CALL EXIT
      END




C     SUBROUTINE DIFFEQ
      SUBROUTINE DIFFEQ (N,X,Y,DY)
      DIMENSION Y(7),DY(7)
      COMMON BETA,M,I,XT,RADT
      COMMON TK,EOT,A,R,ANO,BOLK,G,DELR,XI,DELTAU,AMASS     ,FACTOR
      DIMENSION I(50),XT(50),RADT(50)
      P=Y(5)
      V=Y(6)
      T=Y(7)
```

```
      CALL NOZZLE(X,AC,DADX)
 2000 PLG=9.584586-1648.6068/T-1.638646*T*0.01
    1 +2.403267*T*T*0.00001-1.168708*T*T*T*0.00000001
      PSIN = EXPF(2.3025851*PLG)
      PSIN = 1000.*PSIN
 205  RHO = 235. + 0.654*(TK-T) + 62.77*(TK-T)**0.333333
      RHO = 0.001*RHO
      RHOG=PSIN/(R*T)
      SIGIN = EOT*(TK-T)/(A/RHO)**0.666667
      HFG = 32.938*SQRTF(406.16 - T) - 0.5890*(406.16 - T)
      HFG = 42700.*HFG
      UFG = HFG - PSIN*(1./RHOG - 1./RHO)
      CP = 0.4212 + 0.0151*T/100. + 0.0038051*T*T/10000.
      CP = CP*42700.
      AK = CP/(CP-R)
      IF (P/PSIN-1.0) 300,300,301
 300  AJ=0.0
      RZERO=0.0
      GO TO 60
 301  AM = A/ANO
      AV = AM/RHO
      RM = 0.620351*AV**0.333333
      C1 = 0.797885*(PSIN/T)**2 *AV/BOLK *SQRTF(G/AM)/BOLK
      C2 = 4.18879/(BOLK*T)
      AY = 0.5*RHO*R*T*LOGF(P/PSIN)
      SIG = SIGIN - DELR*RM*AY
      AJ = C1*(P/PSIN)**2 * SQRTF(SIG)*EXPF(-C2*SIG**3/AY**2)
      AJ=AJ*FACTOR
      RSTAR = SIG/A'
      RZERO = 1.3*RSTAR
 60   ALAM = HFG/(CP*T)
      AMACH = V/SQRTF(AK*G*R*T)
      IF(Y(3))70,70,71
 70   RDROP=RZERO
      GO TO 122
 71   RDROP = 3.*AMASS*Y(4)/(RHO*Y(3)'
 122  CALL TEMP(P,T,TD,RDROP)
      DRDX = 1.5*P*R*(TD-T)/(V*UFG*RHO*SQRTF(6.28319*R*T /G))
      DY(1) = 25.13274*AJ*AC
      DY(2) = Y(1)*DRDX + DY(1)*RZERO
      DY(3) = Y(2)*DRDX + 12.56637*AJ*AC*RZERO**2
      DY(4) = RHO*Y(3)*DRDX/AMASS + RHO*AJ*AC*4.1887904*RZERO**3/AMASS
      DY(5) = Y(5)*AK*AMACH**2/(AMACH**2 - 1.) * ((ALAM-1./(1.-Y(4)))
    1          * DY(4) - DADX/AC)
      DY(6) = -Y(6)*DY(5)/(AK*AMACH**2*Y(5))
      DY(7) = Y(7)*(AK-1.)/AK * DY(5)/Y(5) + ALAM*DY(4) *Y(7)
      RETURN
      END



 C    SUBROUTINE NOZZLE FOR SQUARED NOZZLES
      SUBROUTINE NOZZLE (X,AC,DADX)
      COMMON BETA
```

```
      IF (X-2.540) 11,12,12
   11 ROOT=SQRTF(5.(8*X-X*X)
      AC=2.770-1.016*ROOT
      DADX=-1.016*(2.54-X)/ROOT
      GO TO 300
   12 ASIN=SINF(BETA)
      IF (X-2.540-2.540*ASIN) 11,21,21
   21 ACOS=COSF(BETA)
     0AC=0.1885+2.581*(1.-ACOS) +
    1  1.016*(X-(2.540+2.540*ASIN))*ASIN/ACOS
      DADX=1.016*ASIN/ACOS
  300 RETURN
      END
```

C   SUBROUTINE NOZZLE FOR CORRECTED NOZZLES

```
      SUBROUTINE NOZZLE(X,AC,DADX)
      COMMON BETA
      AK=1.31
      ASTAR=BETA
      A1=(AK-1.)/AK
      A2=(2.*AK-1.)/AK
      A3=(AK+1.)/(2.*AK-2.)
      A4=(3.-AK)/(2.*AK-2.)
      CALL TABLE(X,RAD,DRAD)
      AMACH=SQRTF(2.*(1./RAD**A1-1.)/(AK-1.))
      DMACH=-DRAD/(AK*AMACH*RAD**A2)
      B=(2.+(AK-1.)*AMACH*AMACH)/(AK+1.)
      AC=ASTAR/AMACH*B**A3
      DADX=ASTAR*DMACH*(B**A4-B**A3/(AMACH*AMACH))
      RETURN
      END
```

C   SUBROUTINE TABLE

```
      SUBROUTINE TABLE (X,RAD,DRAD)
      COMMON BETA,M,I,XT,RADT
      DIMENSION I(50),XT(50),RADT(50)
      I=1
   70 IF (X-XT(I)) 71,72,73
   72 RAD=RADT(I)
      X1=XT(I)
      X2=XT(I+1)
      RAD2=RADT(I+1)
      DRAD=(RAD2-RAD)/(X2-X1)
      GO TO 69
   73 X1=XT(I)
      RAD1=RADT(I)
      I=I+1
      GO TO 70
   71 X2=XT(I)
      RAD2=RADT(I)
      DRAD=(RAD2-RAD1)/(X2-X1)
```

```
      RAD=RAD1+DRAD*(X-X1)  .
   69 CONTINUE
      RETURN
      END




C      SUBROUTINE TEMP
       SUBROUTINE TEMP(P,T,TD,RDROP)
       COMMON BETA,M,I,XT,RADT
       COMMON TK,EOT,A,R,ANO,BOLK,G,DELR,XI,DELTAU,AMASS
       DIMENSION I(50),XT(50),RADT(50)
       DELTA=100.*DELTAU
       T1=T
       T2=T
       TAU=1.
 2000PLG=9.584586-1648.6068/T-1.638646*T*0.01
    1 +2.403267*T*T*0.00001-1.168708*T*T*T*0.00000001
      PSIN = EXPF(2.302585;*PLG)
      PSIN = 1000.*PSIN
 205  RHO = 235. + 0.654*(TK-T) + 62.77*(TK-T)**0.333333
      RHO = 0.001*RHO
      RHOG=PSIN/(R*T)
      SIGIN = EOT*(TK-T)/(A/RHO)**0.666667
      HFG = 32.938*SQRTF(406.16 - T) - 0.5890*(406.16 - T)
      HFG = 42700.*HFG
      UFG = HFG - PSIN*(1./RHOG - 1./RHO)
 301  AM = A/ANO
      AV = AM/RHO
      RM = 0.620351*AV**0.333333
      SIG=SIGIN/(1.+DELR*RM/RDROP)
 122  B1 = 0.666667*UFG*XI/(R*T)
      B2 = 2.*SIG/(RHO*R*T*RDROP)
  20  PI=(1. ,TAU-1.)/B1)*SQRTF(TAU)/EXPF(B2/TAU)
      PSINDR=PI*P
      CALL SAT(PSINDR,TDR)
      T=TDR
      IF(ABSF(T2-TDR)-DELTA) 2,2,1
    1 T2=TDR
      TAU=TDR/T1
      GO TO200
    2 TD=TDR
      T=T1
      RETURN
      END




C      SUBROUTINE SAT
       SUBROUTINE SAT(PSINDR,TDR)
       T=20.0
       DELT=50.0
       DELTDR=0.0001
       PSIN=PSINDR/1000.
       PLGDR=0.434294*LOGF(PSIN)
```

```
2000PLG=9.584586-1648.6068/T-1.638646*T*0.01
   1 +2.403267*T*T*0.00001-1.168708*T*T*T*0.00000001
     IF (PLG-PLGDR) 10,22,30
  10 A=T
     T=T+DELT
     GO TO 200
  30 B=T
 300 T=0.5*(A+B)
12000PLG=9.584586-1648.6068/T-1.638646*T*0.01
   1 +2.403267*T*T*0.00001-1.168708*T*T*T*0.00000001
     0DPLG=1648.6068/(T*T)-0.01638646
   1   +2.403267*0.00002*T-1.168708*0.00000003*T*T
     TI=T-(PLG-PLGDR)/DPLG
     IF(ABSF(TI-T)-DELTDR) 20,20,21
  21 T=TI
     GO TO 1200
  20 T=TI
  22 TDR=T
     RETURN
     END
```
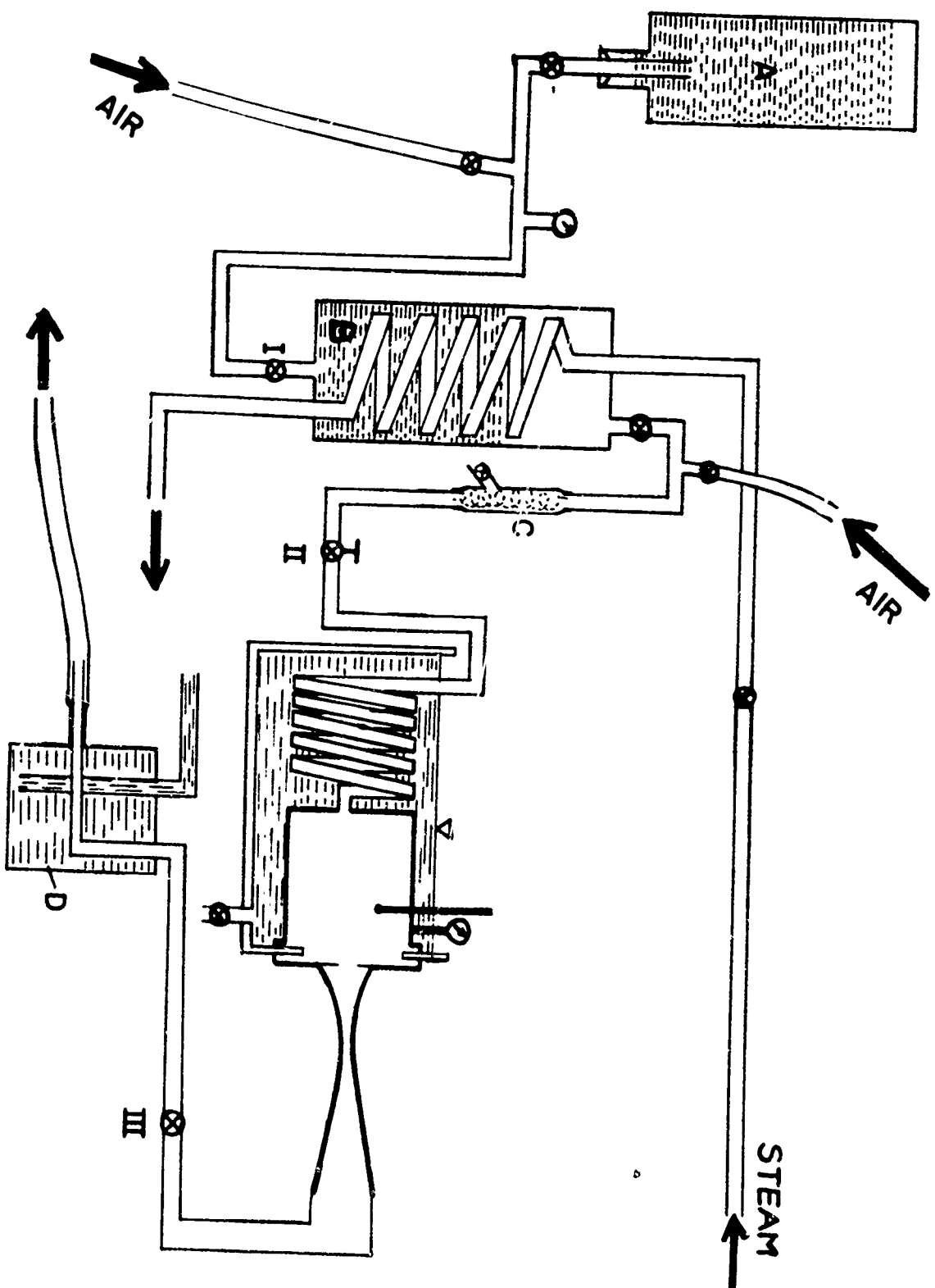
FIG. Ia SCHEMATIC OF APPARATUS
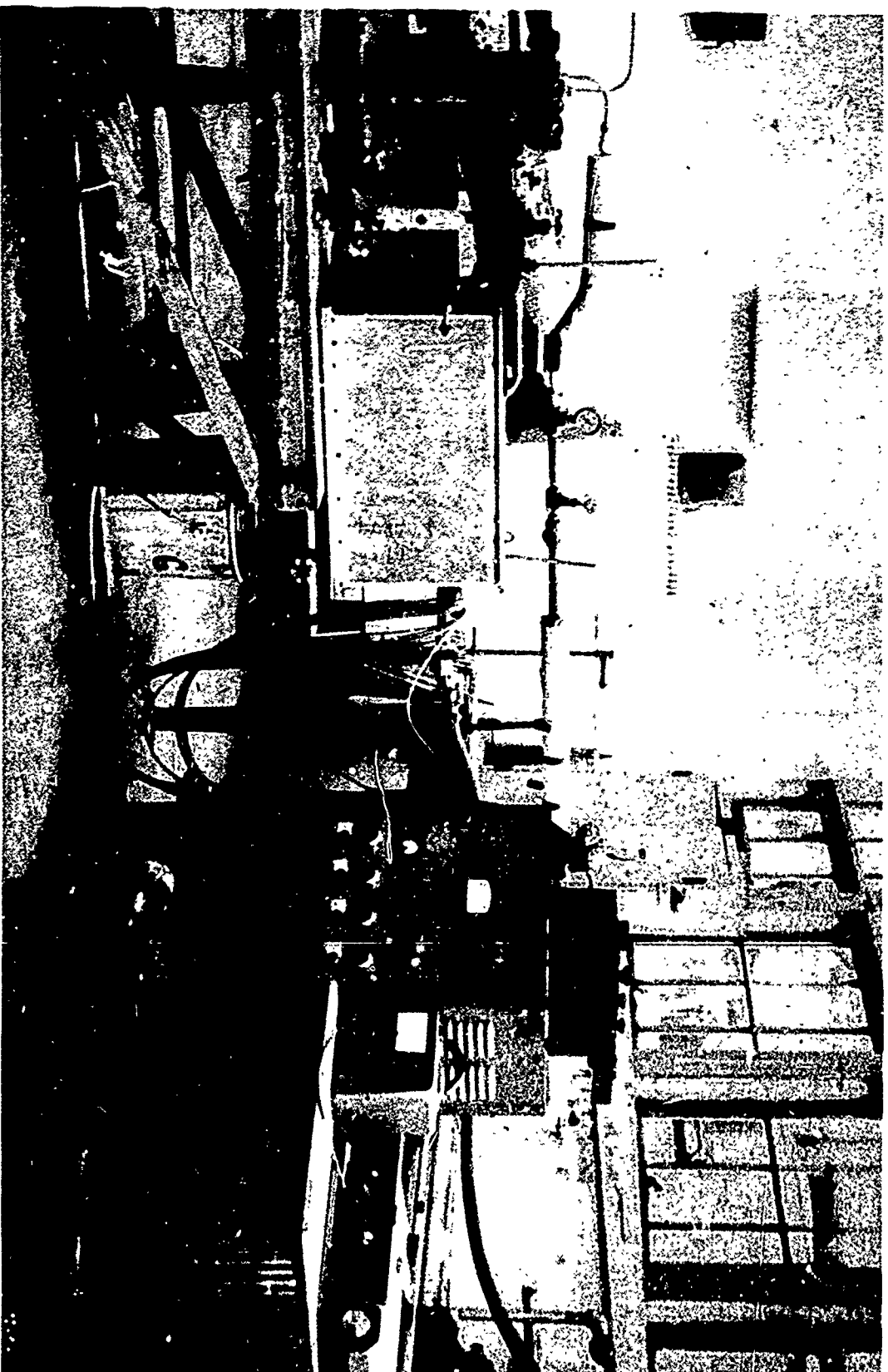
FIG 1b EXPERIMENTAL EQUIPMENT
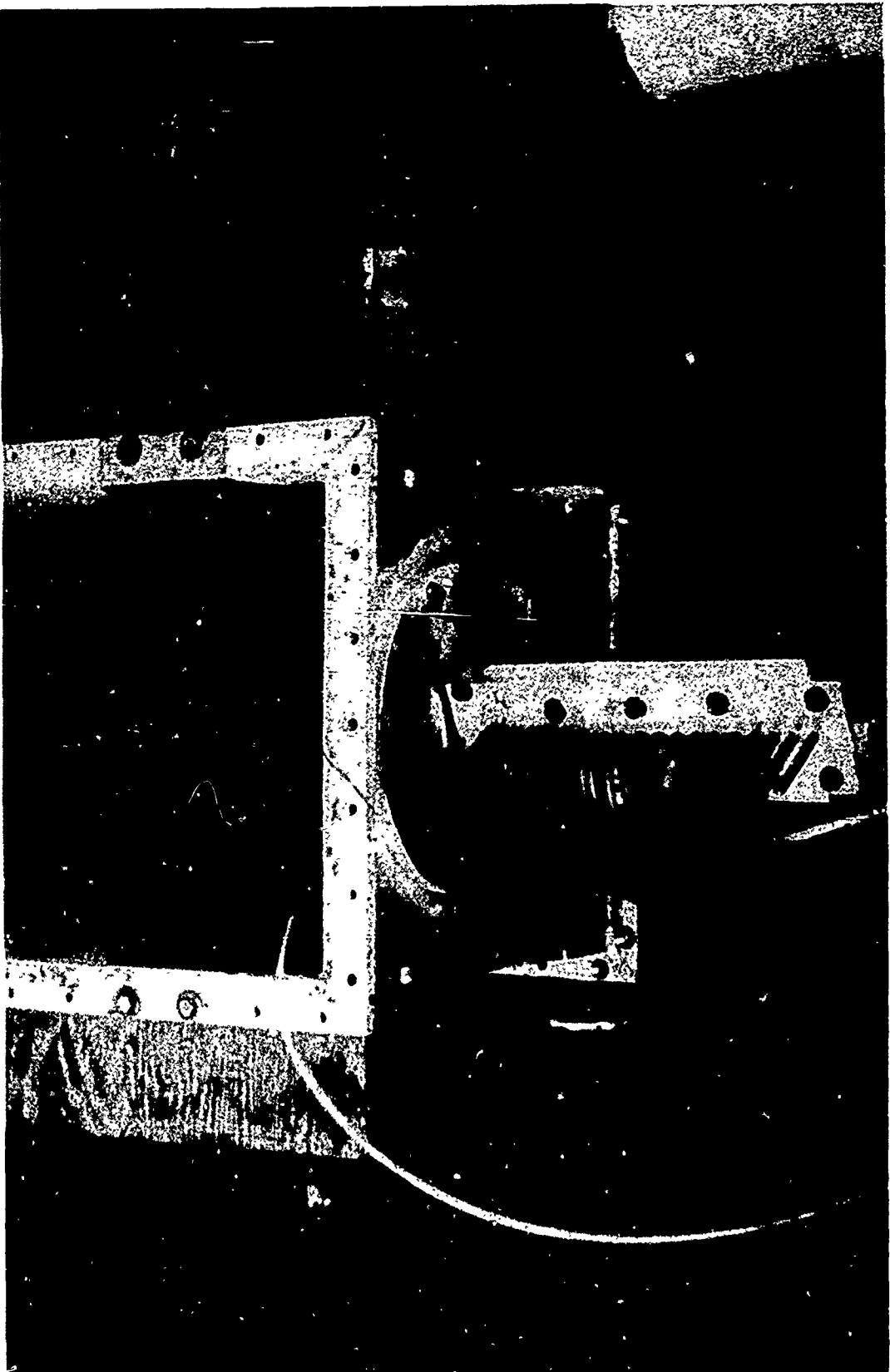
TEMPERATURE BATH AND 2-DIM·NOZZLE·

FIG 2a
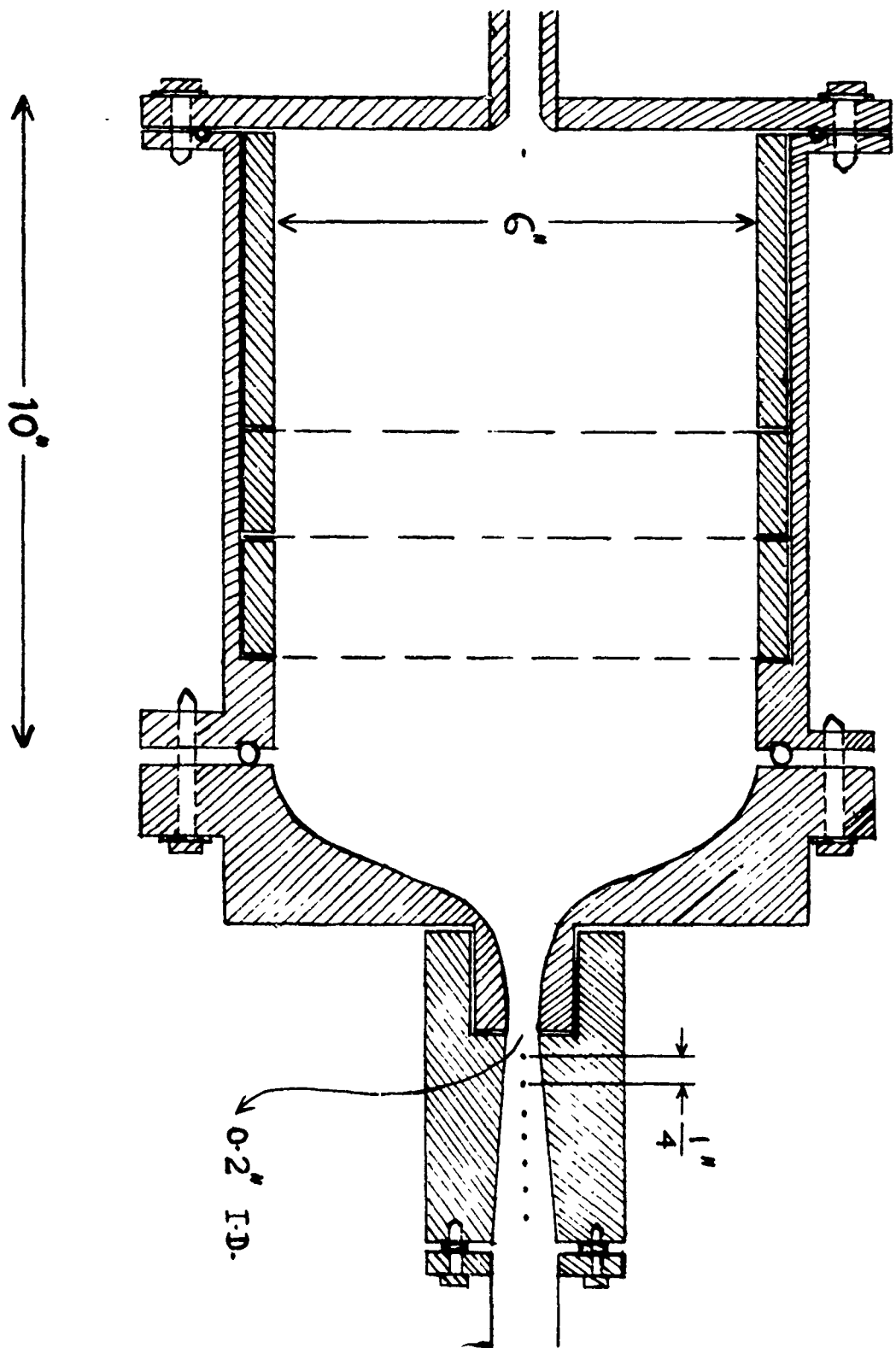
FIG. 2b SCHEMATIC OF STAGNATION TANK AND AXi−SYMMETRIC
NOZZLE PROFILE.

STAGNATION TANK

0.146"

1" RADIUS

9"

1/4"

0.020"

0.200"

1/2"
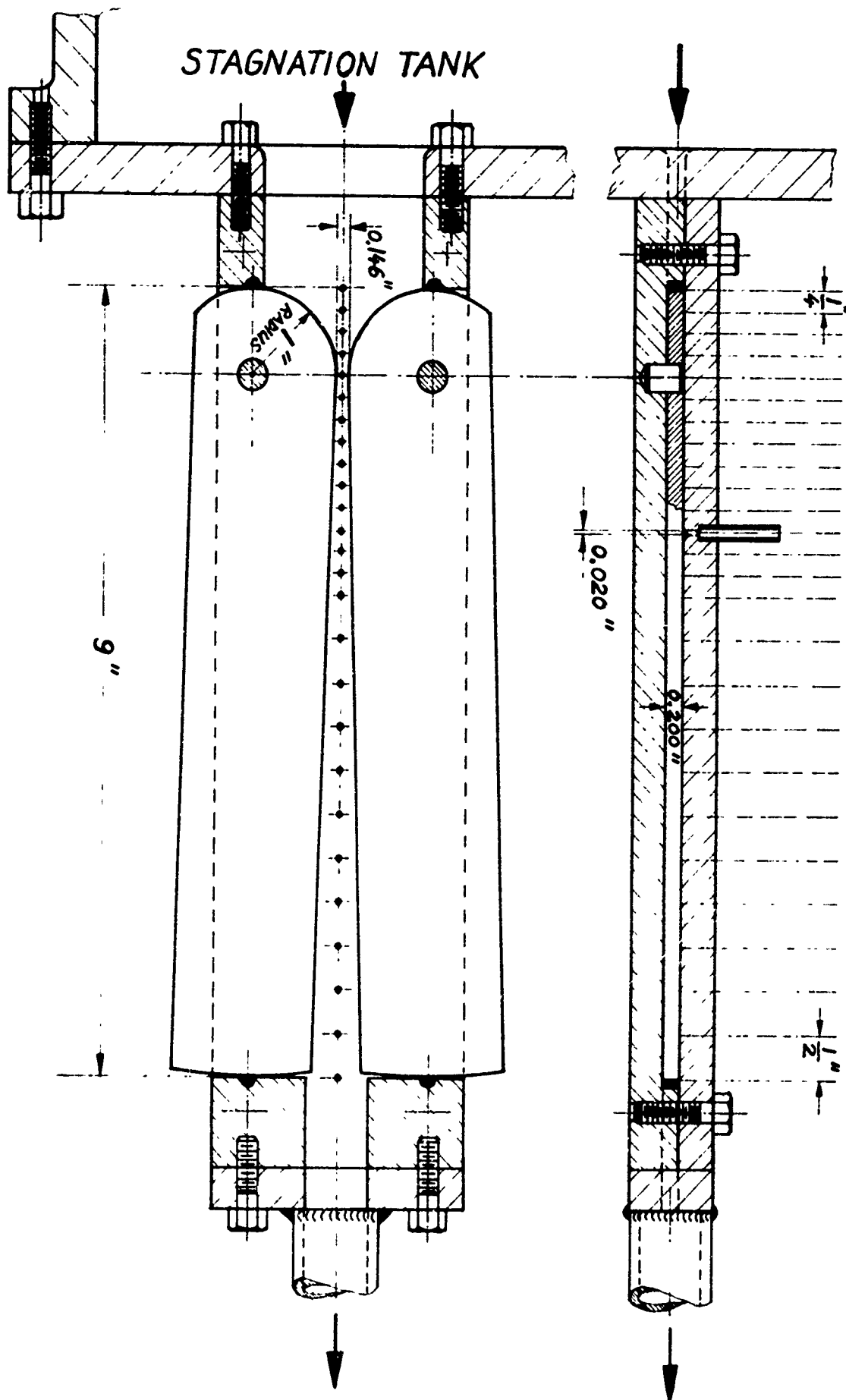
FIG. 3   2-DIMENSIONAL NOZZLE PROFILE
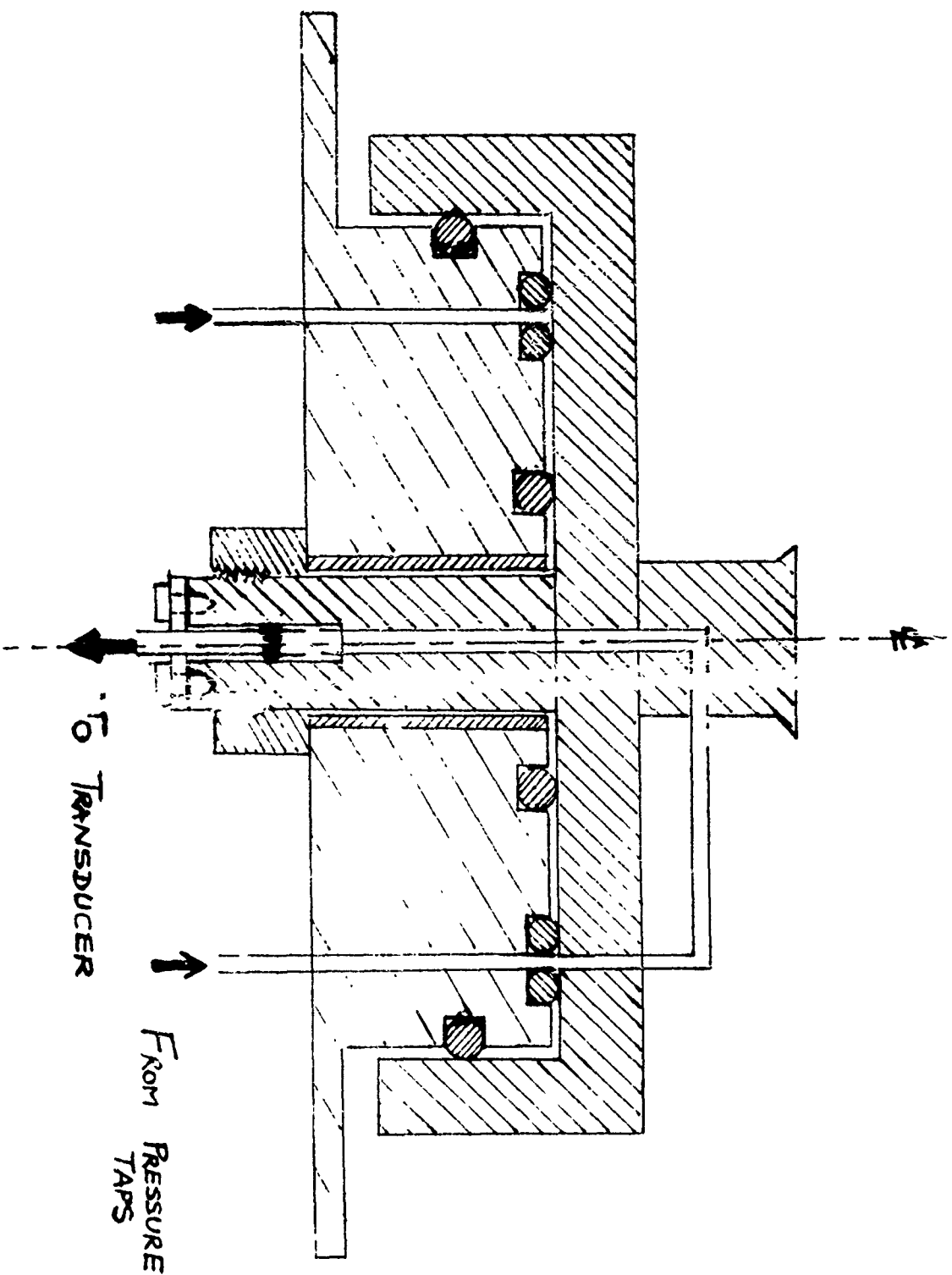
FIG. 4 ROTARY PRESSURE SWITCH DEVICE

TO TRANSDUCER

FROM PRESSURE TAPS
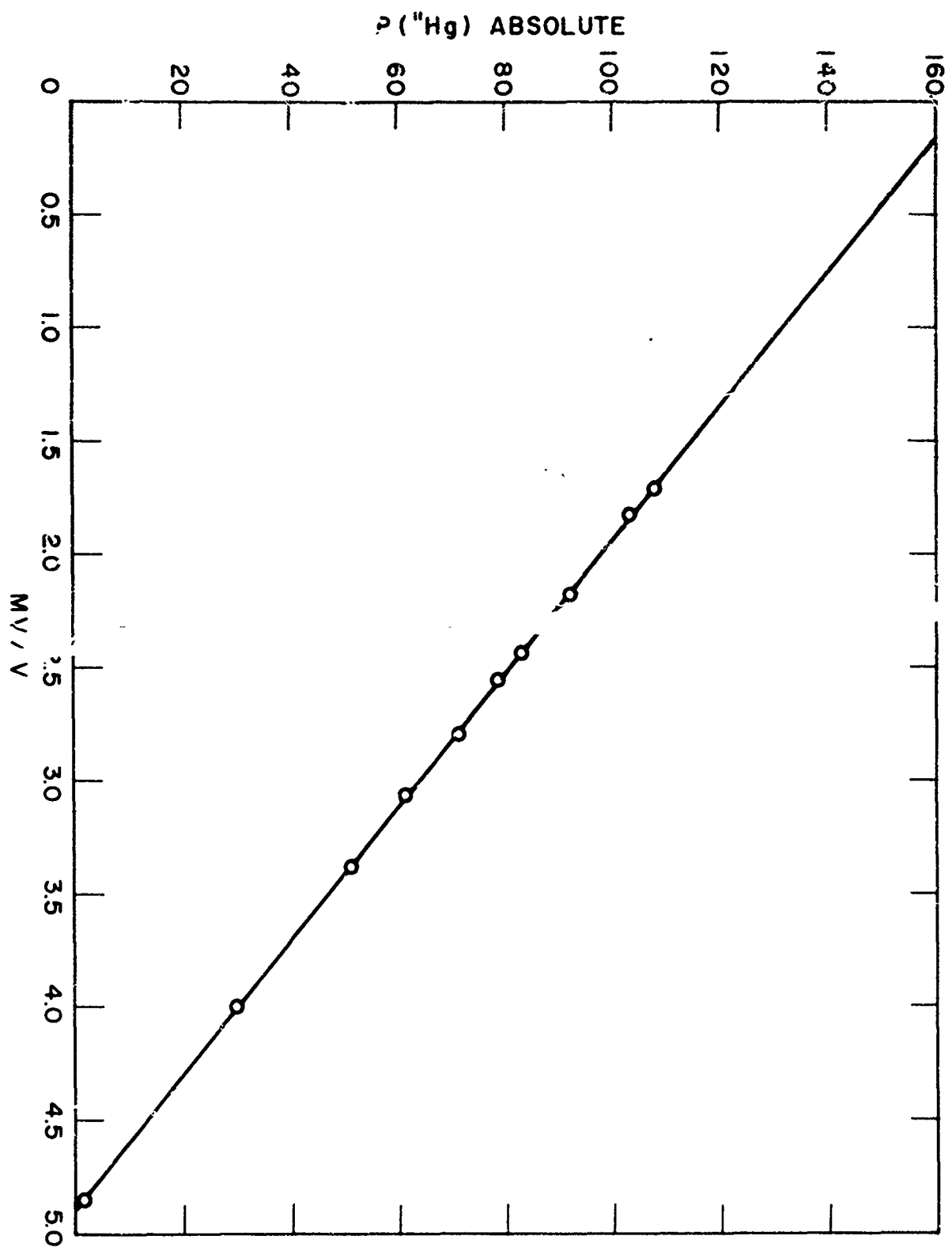
FIG. 5 TRANSDUCER CALIBRATION, ILLUSTRATING LINEAR CHARACTERISTIC

FIG. 6 PRESSURE DISTRIBUTON ON – AXI–SYMMETRIC NOZZLE

P / P₀₁

A/A*

$\overline{P}_0$ = 47.2 psia
T_0 = 62°F

EXPERIMENTAL

ISENTROPIC

THEORETICAL
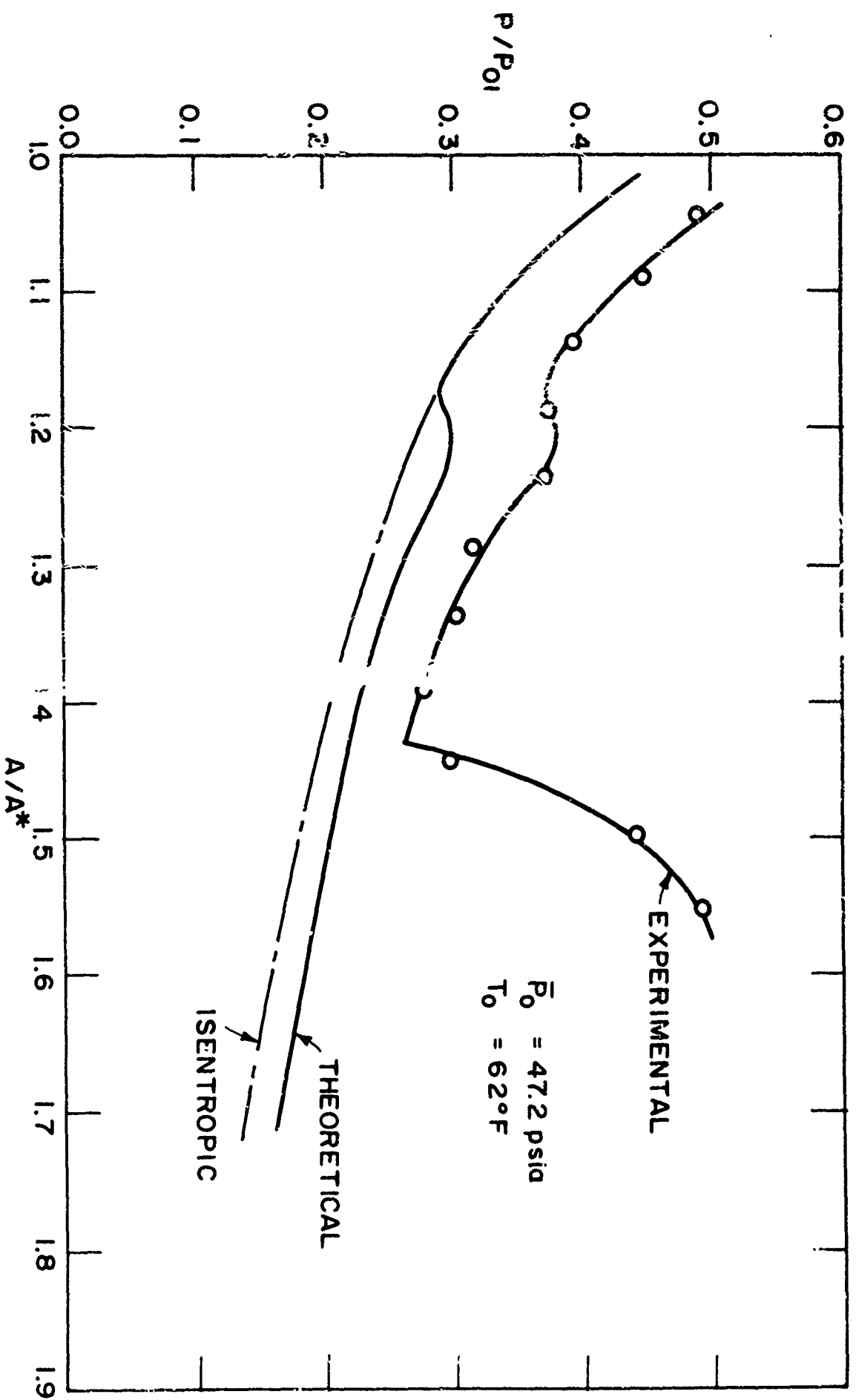
FIG. 7 PRESSURE DISTRIBUTION - AXI-SYMMETRIC NOZZLE
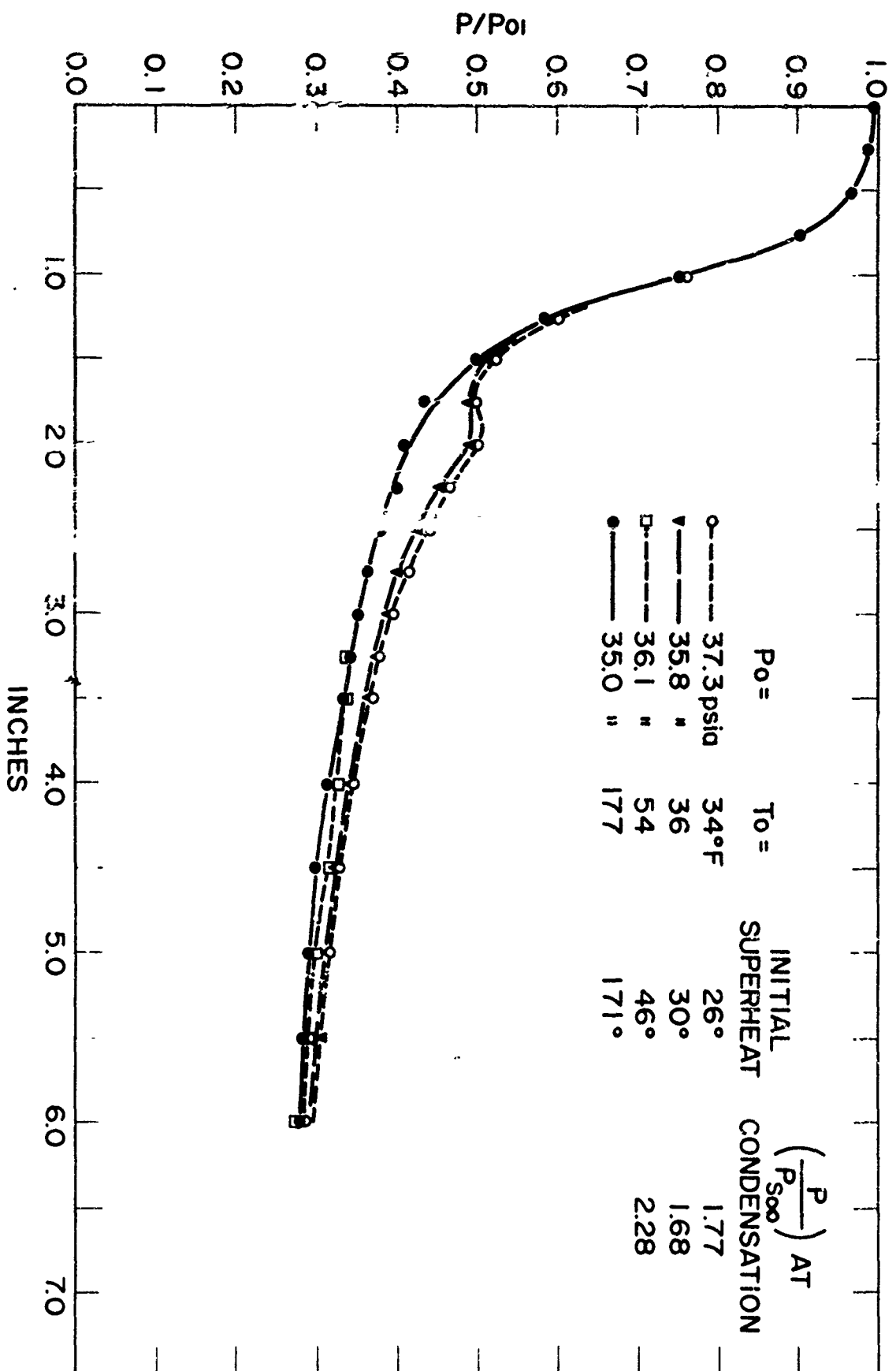
EXPERIMENTAL

○ $P_0 = 53.9$ psia
  $T_0 = 77°F$

▼ $P_0 = 67.4$
  $T_0 = 47$

THEORETICAL

ISENTROPIC

P/P$_{01}$

A/A*

FIG. 8 PRESSURE DISTRIBUTIONS, CONTINUED, 2-DIMENSIONAL NOZZLE (1° INCLUDED ANGLE)
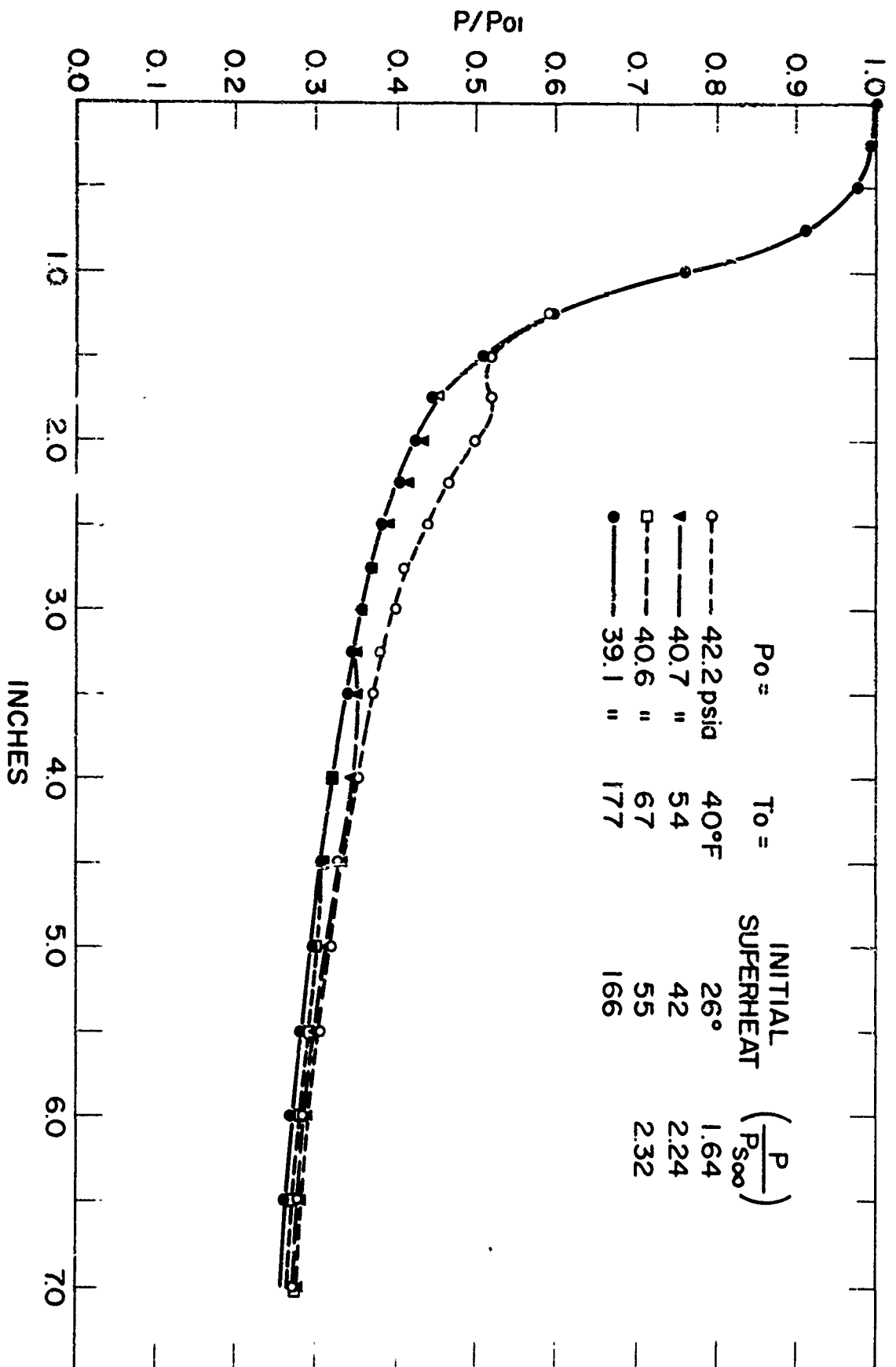
Legend (within figure):

	Po =	To =	INITIAL SUPERHEAT	$\left(\dfrac{P}{P_{S\infty}}\right)$ AT CONDENSATION
○-----	37.3 psia	34°F	26°	1.77
▼———	35.8 "	36	30°	1.68
□-----	36.1 "	54	46°	2.28
●———	35.0 "	177	171°	

FIG. 9 PRESSURE DISTRIBUTIONS, CONTINUED, 2-DIMENSIONAL NOZZLE (1° INCLUDED ANGLE)

P/Po1

	Po =	To =	INITIAL SUPERHEAT	$\left(\dfrac{P}{P_{s\infty}}\right)$
o——————	42.2 psia	40°F	26°	1.64
▼—————	40.7 "	54	42	2.24
□—————	40.6 "	67	55	2.32
●—————	39.1 "	177	166	

INCHES

P/Po1

GEOMETRIC
THROAT

	Po =	To =	INITIAL SUPERHEAT	$\left(\dfrac{P}{P_{s\infty}}\right)$
○———	46.9psia	40°F	21°	1.59
▼———	47.0 "	54	35°	2.43
□———	45.7 "	55	38°	2.90
◇———	44.8 "	67	50°	2.90
●———	45.2 "	174	157°	2.47

0.0 0.1 0.2 0.3 0.4 0.5 0.6 0.7 0.8 0.9 1.0

1.0   2.0   3.0   4.0   5.0   6.0   7.0
INCHES
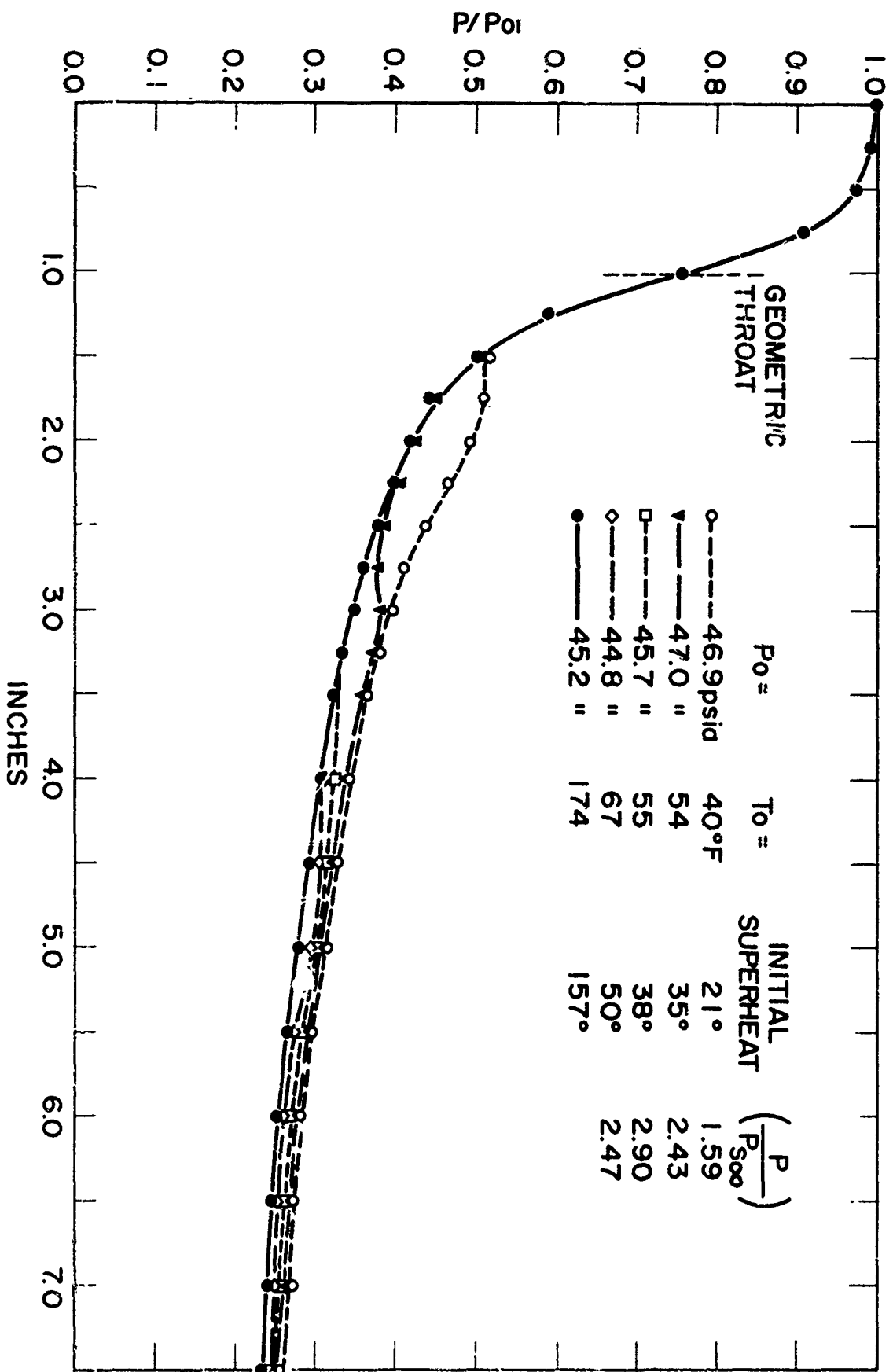
FIG. 10 PRESSURE DISTRIBUTIONS, CONTINUED, 2-DIMENSIONAL NOZZLE (1° INCLUDED ANGLE)
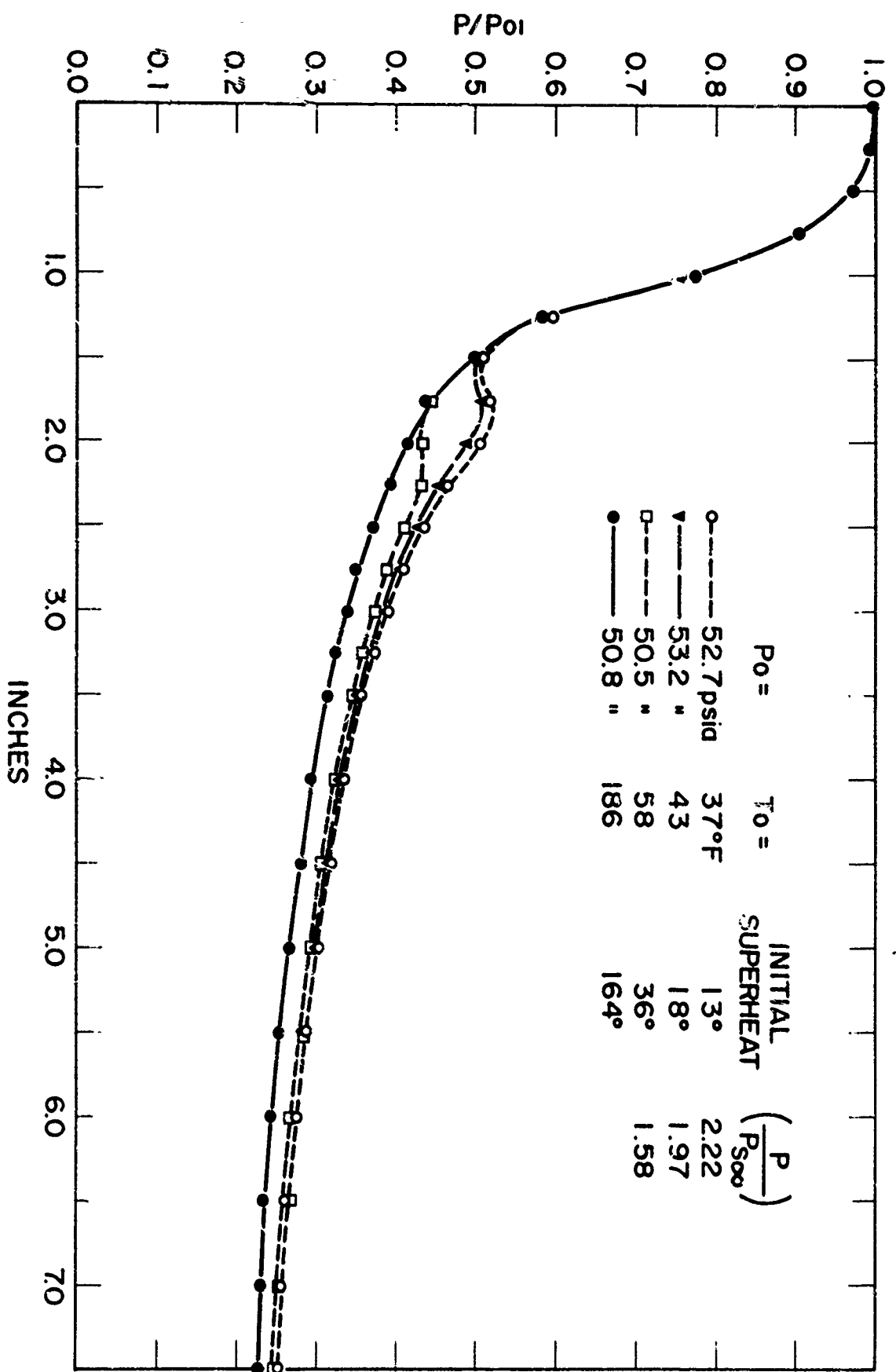
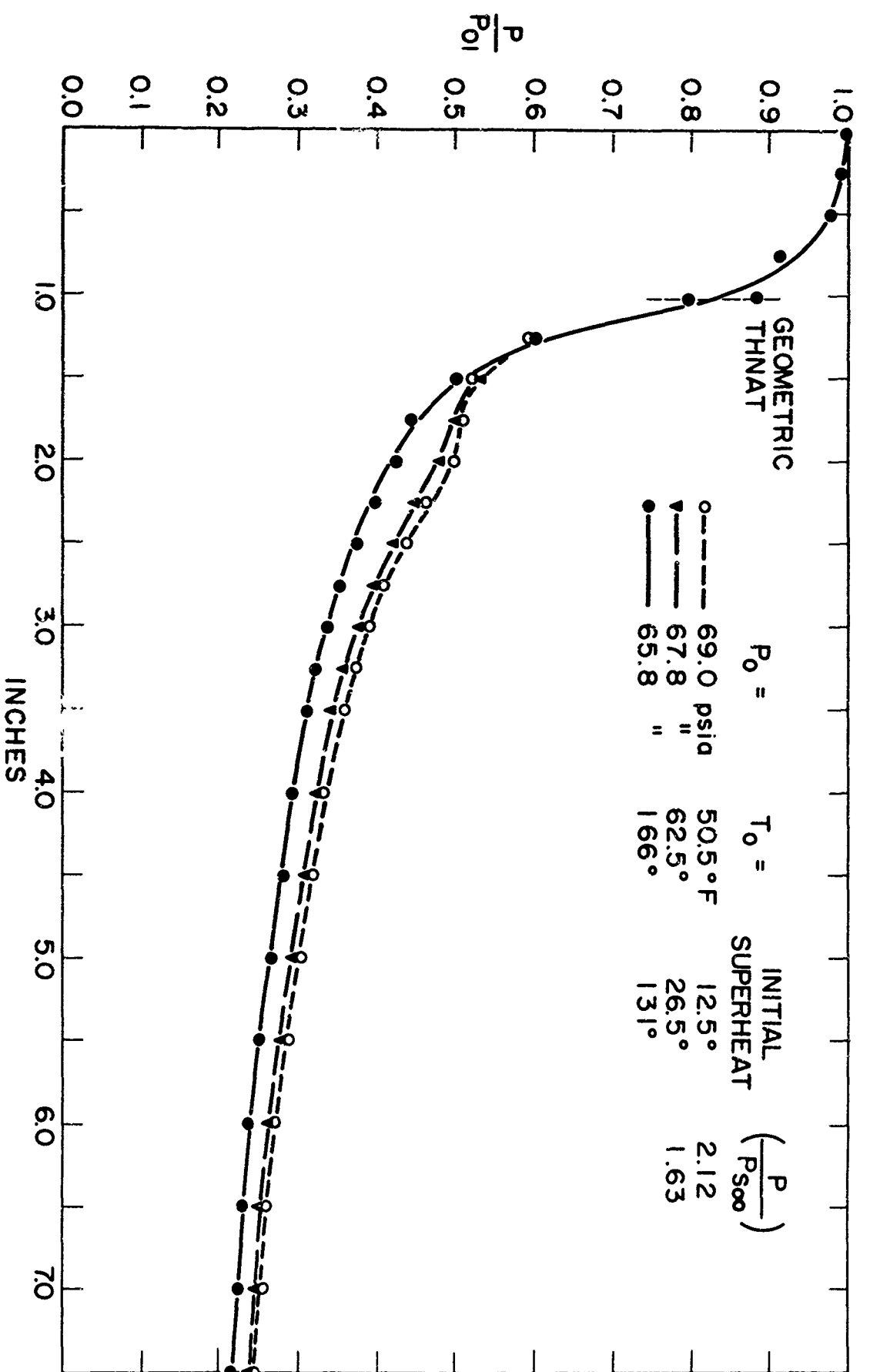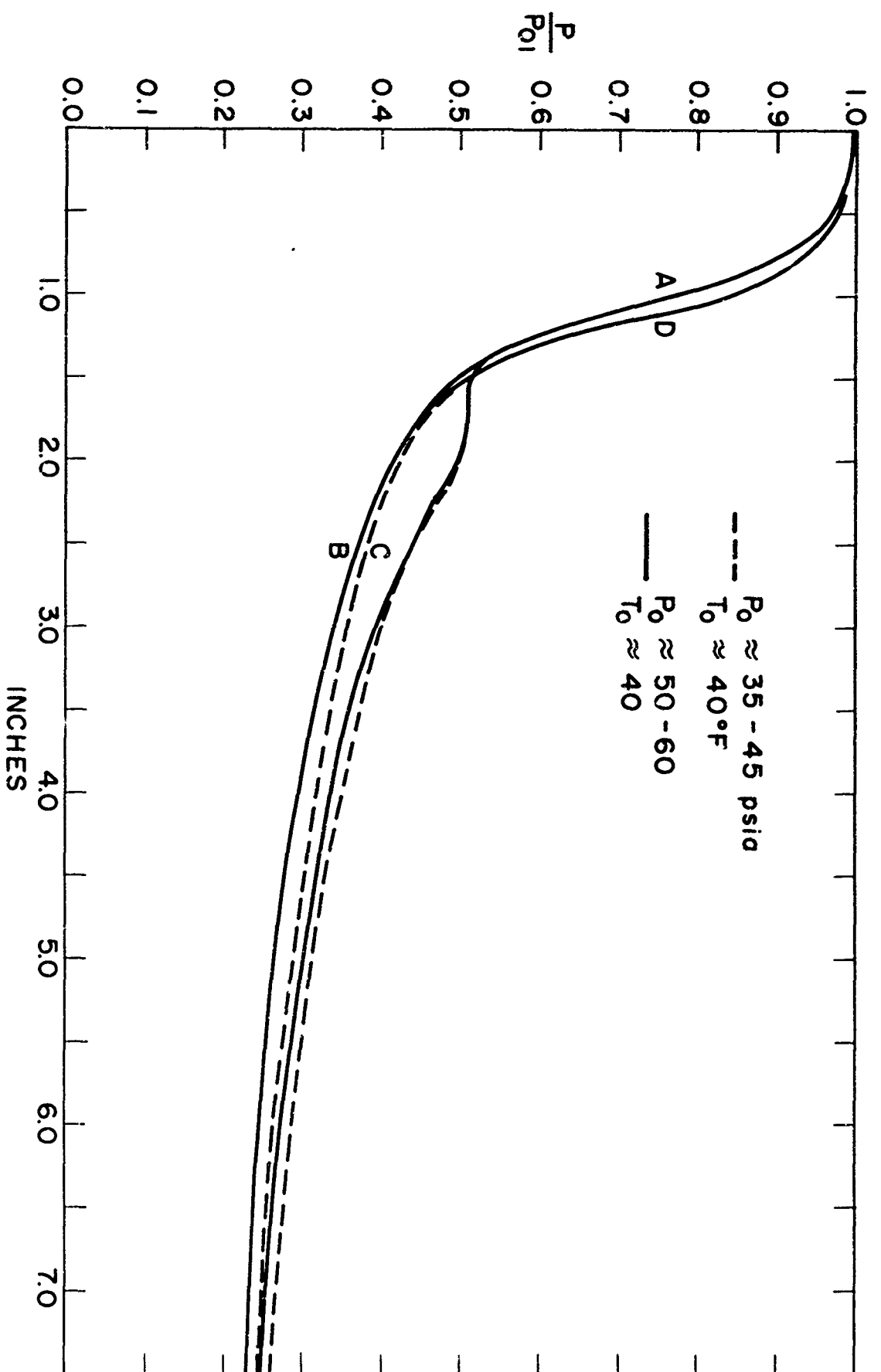FIG. 11 PRESSURE DISTRIBUTIONS, CONTINUED, 2-DIMENSIONAL NOZZLE (1° INCLUDED ANGLE)
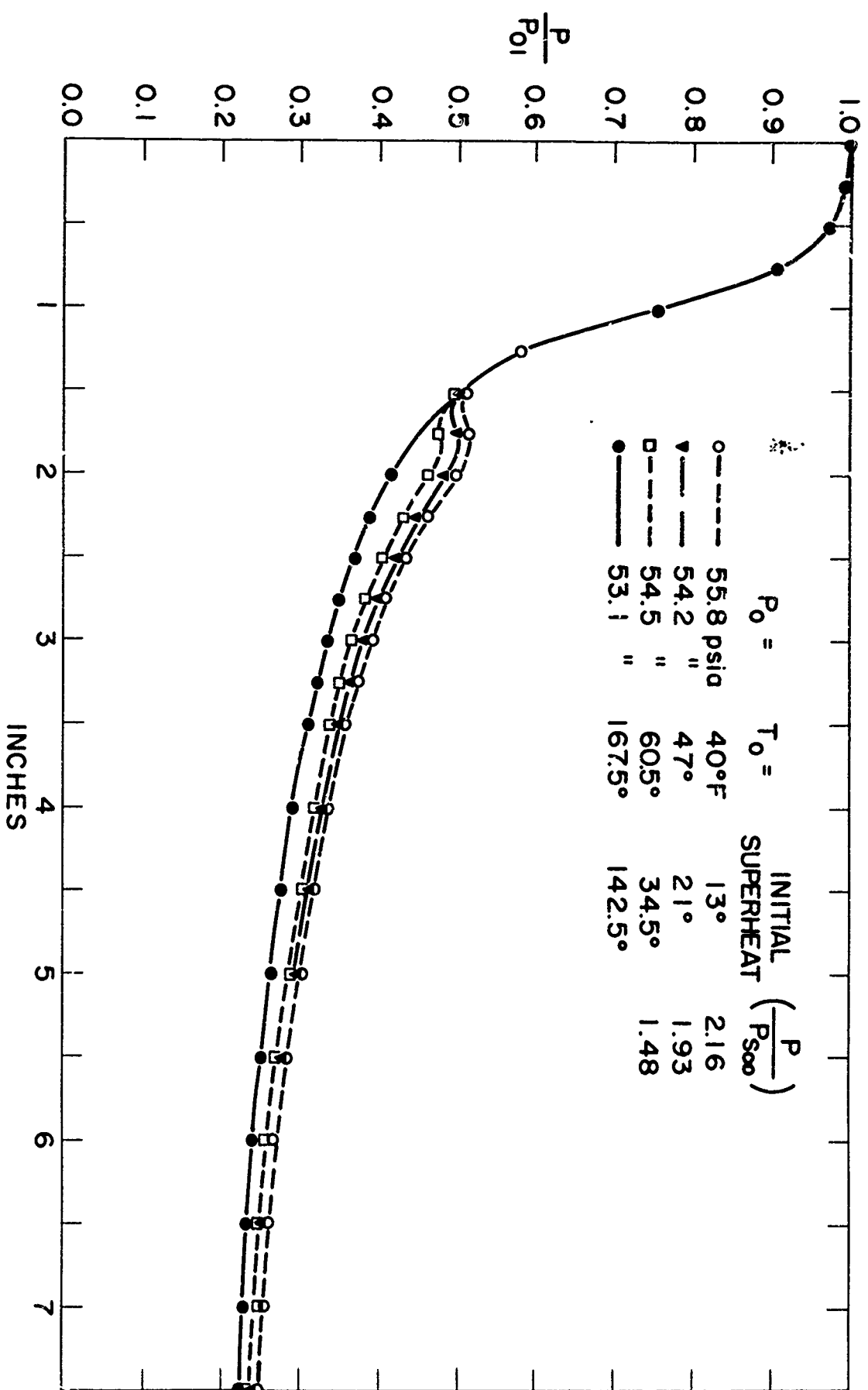
FIG. 12 PRESSURE DISTRIBUTIONS, CONTINUED, 2-DIMENSIONAL NOZZLE (1° INCLUDED ANGLE)

	$P_o =$	$T_o =$	INITIAL SUPERHEAT	$\left(\dfrac{P}{P_{soo}}\right)$
○————	55.8 psia	40°F	13°	2.16
▼———	54.2 "	47°	21°	1.93
□—————	54.5 "	60.5°	34.5°	1.48
●———	53.1 "	167.5°	142.5°	1.48

$\dfrac{P}{P_{OI}}$

INCHES
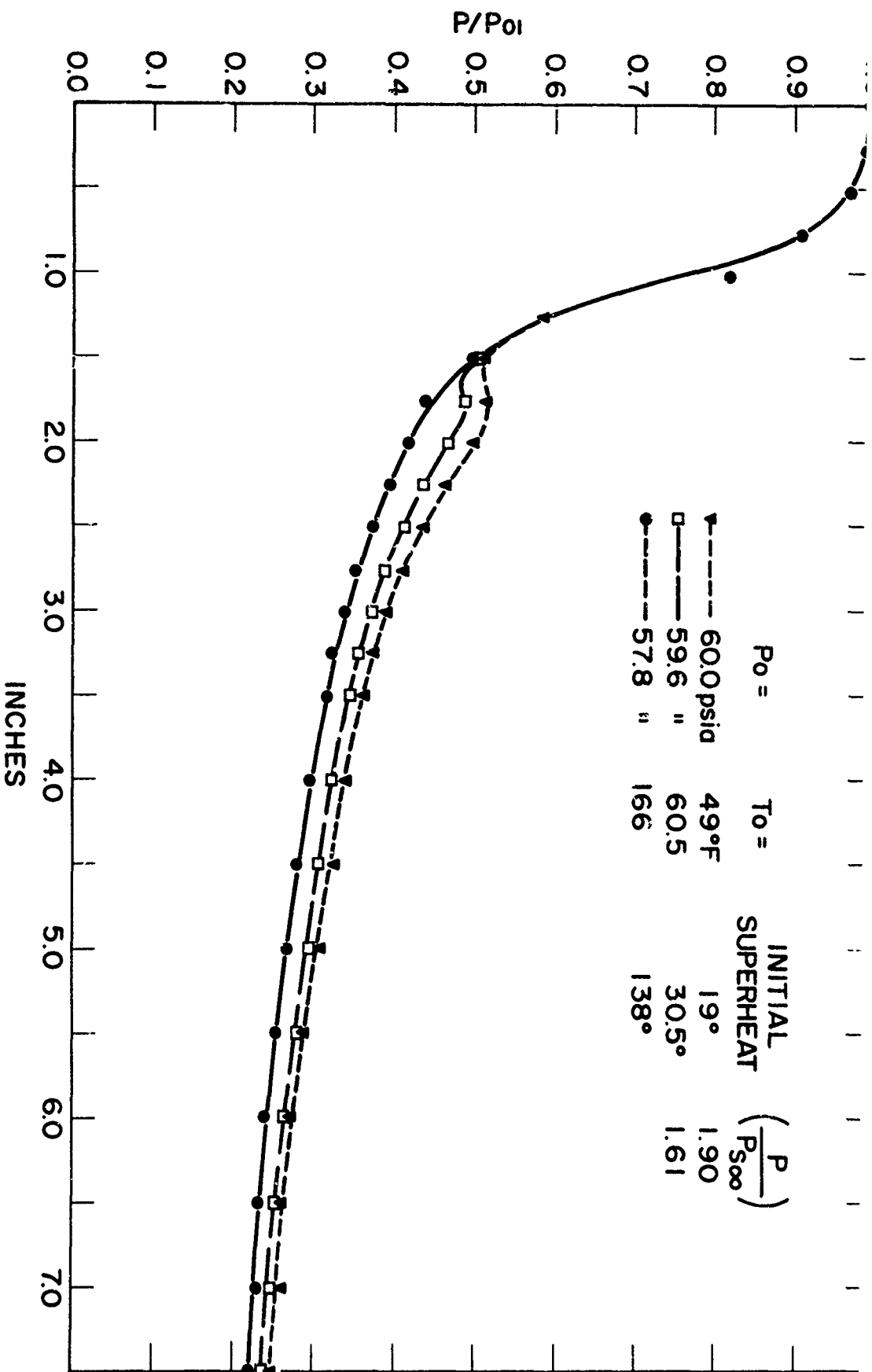
FIG. 13 PRESSURE DISTRIBUTIONS, CONTINUED, 2-DIMENSIONAL NOZZLE (1° INCLUDED ANGLE)
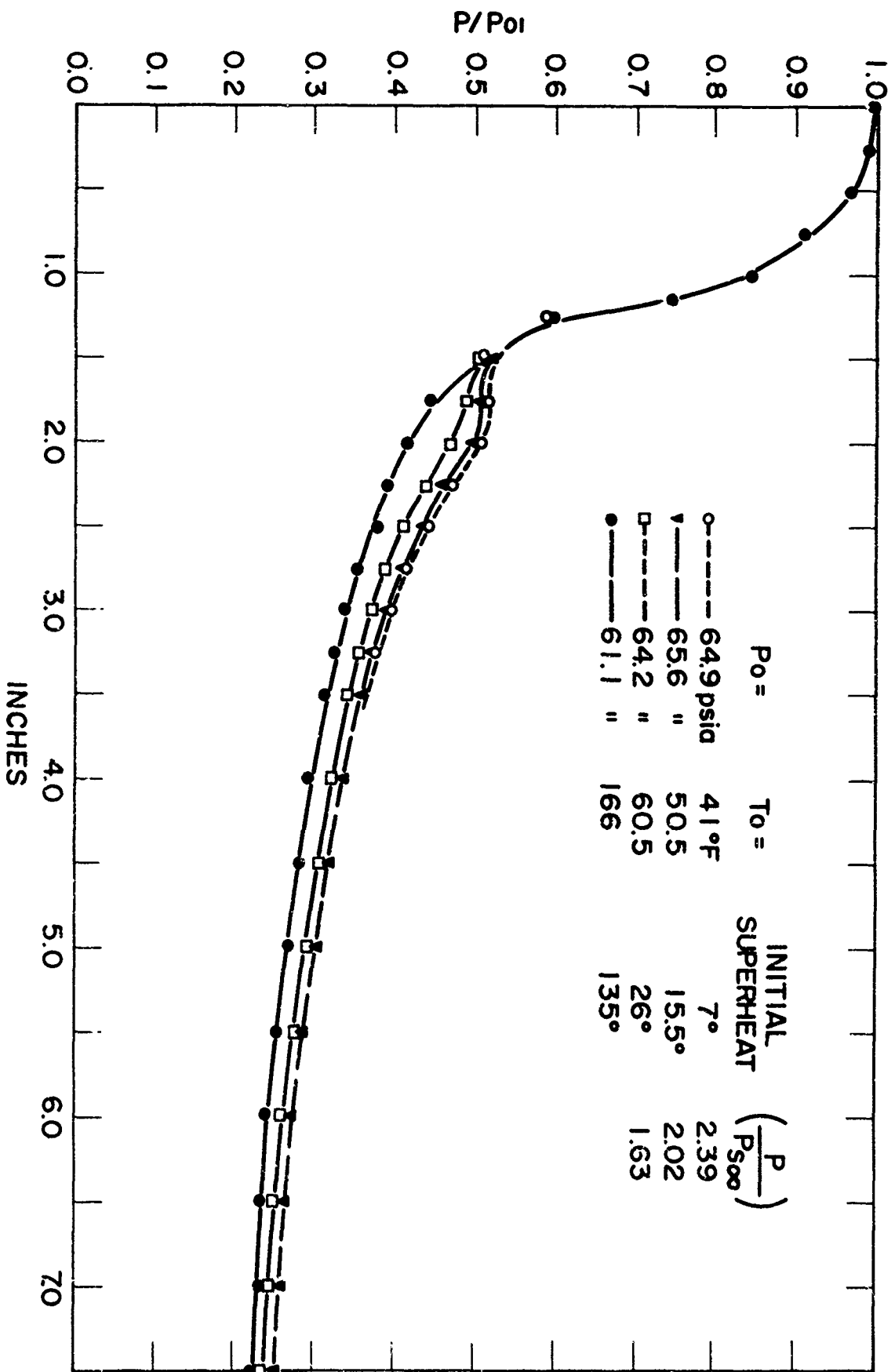
FIG. 14 PRESSURE DISTRIBUTIONS, CONTINUED, 2-DIMENSIONAL NOZZLE (1° INCLUDED ANGLE)
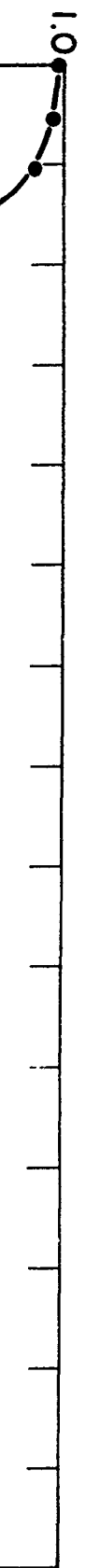
FIG. 15 PRESSURE DISTRIBUTIONS, CONTINUED, 2-DIMENSIONAL NOZZLE (1° INCLUDED ANGLE)

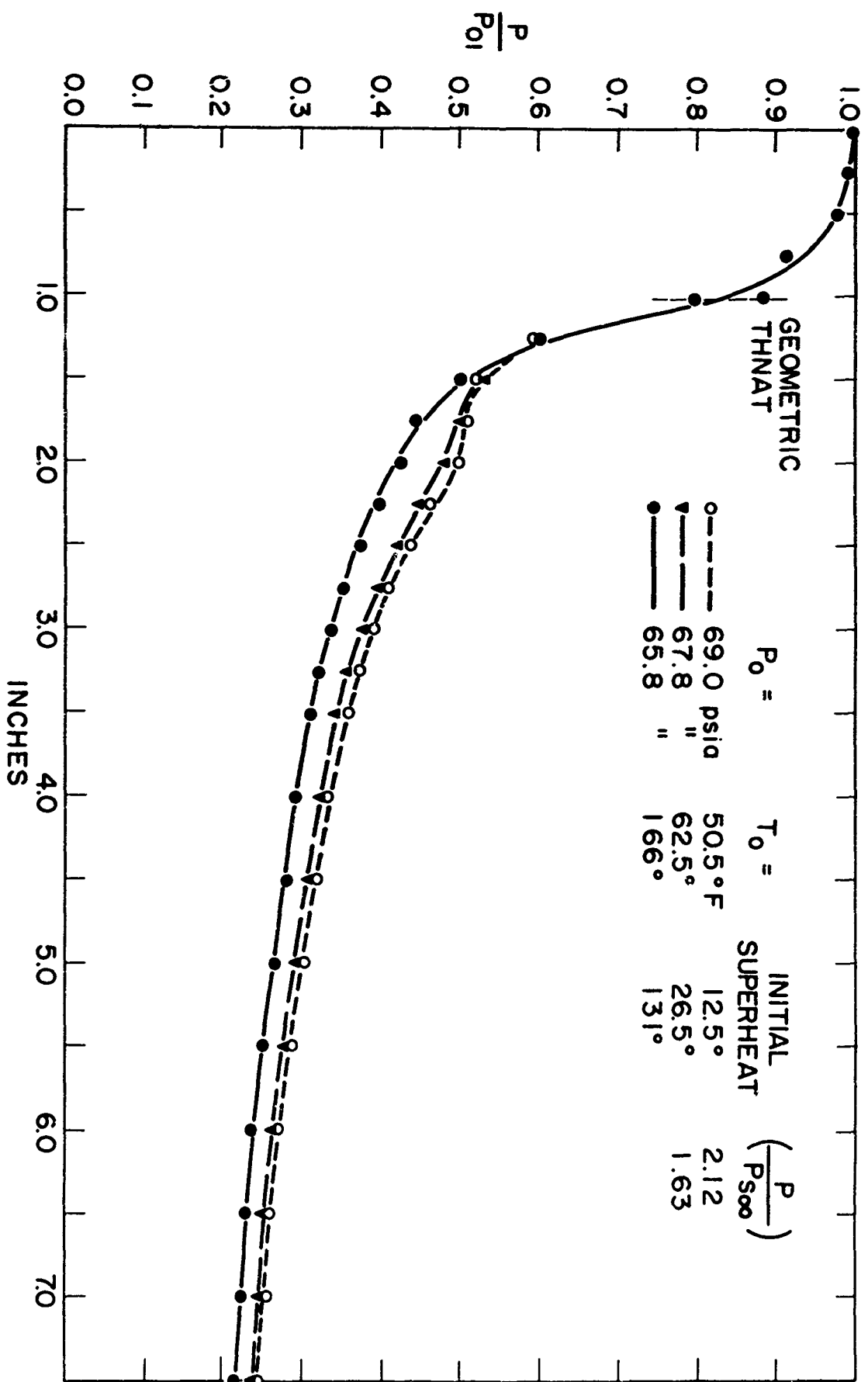FIG. 16 EFFECT OF P_0 ON NON-CONDENSING PRESSURE DISTRIBUTION

$\frac{P}{P_{01}}$

A

D

B

C

$P_0 \approx 35 - 45$ psia
$T_0 \approx 40°F$

$P_0 \approx 50 - 60$
$T_0 \approx 40$

INCHES

FIG. 15 PRESSURE DISTRIBUTIONS, CONTINUED, 2-DIMENSIONAL NOZZLE (1° INCLUDED ANGLE)

FIG. 16 EFFECT OF P_0 ON NON-CONDENSING PRESSURE DISTRIBUTION

Legend (within figure):

$\dfrac{P}{P_{0i}}$

INCHES

- - - $P_0 \approx 35 - 45$ psia, $T_0 \approx 40°F$
—— $P_0 \approx 50 - 60$, $T_0 \approx 40$

A D

B C
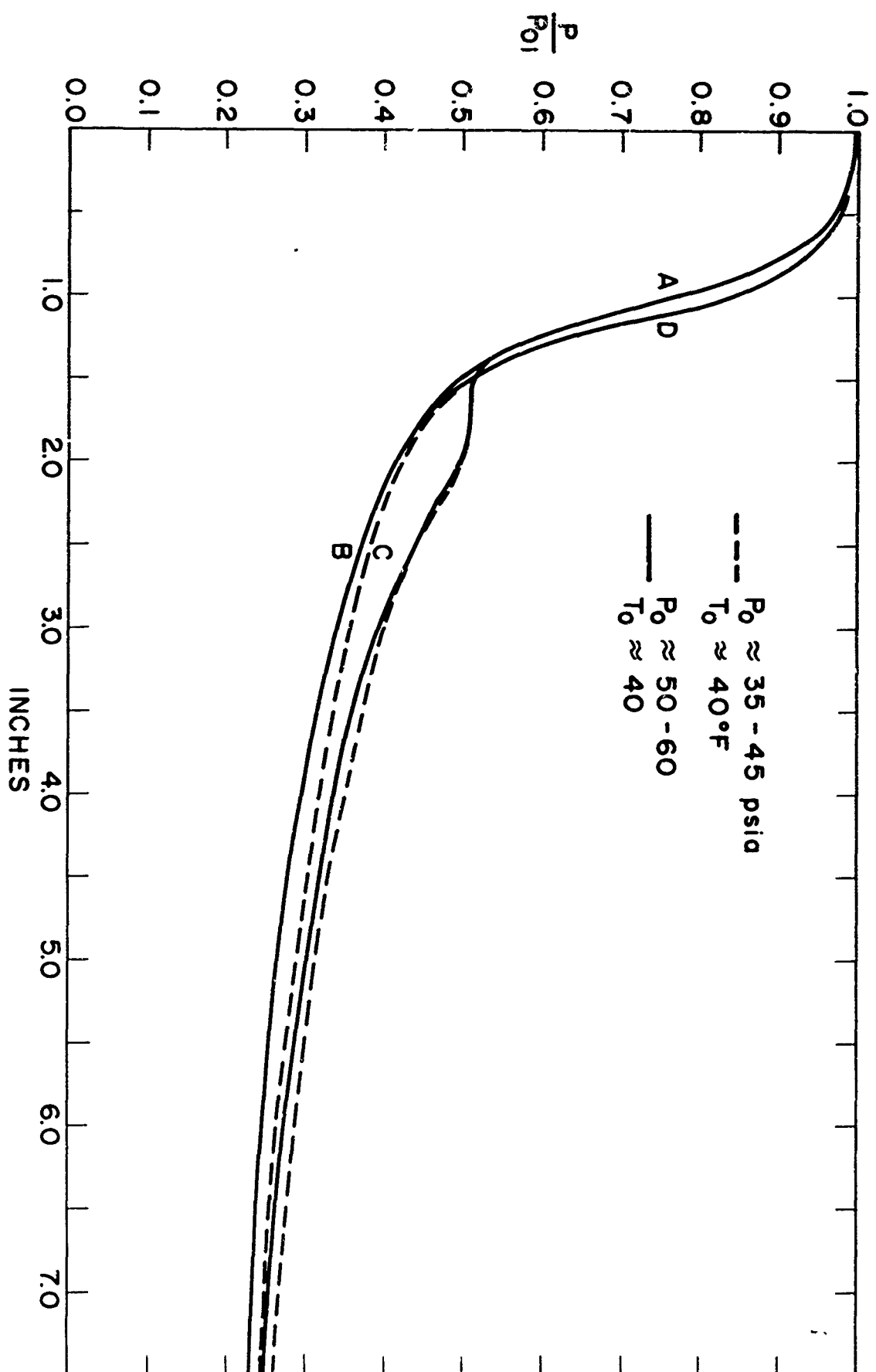
FIG. 17 PRESSURE DISTRIBUTIONS - 2 - DIMENSIONAL NOZZLE (3° INCLUDED ANGLE)

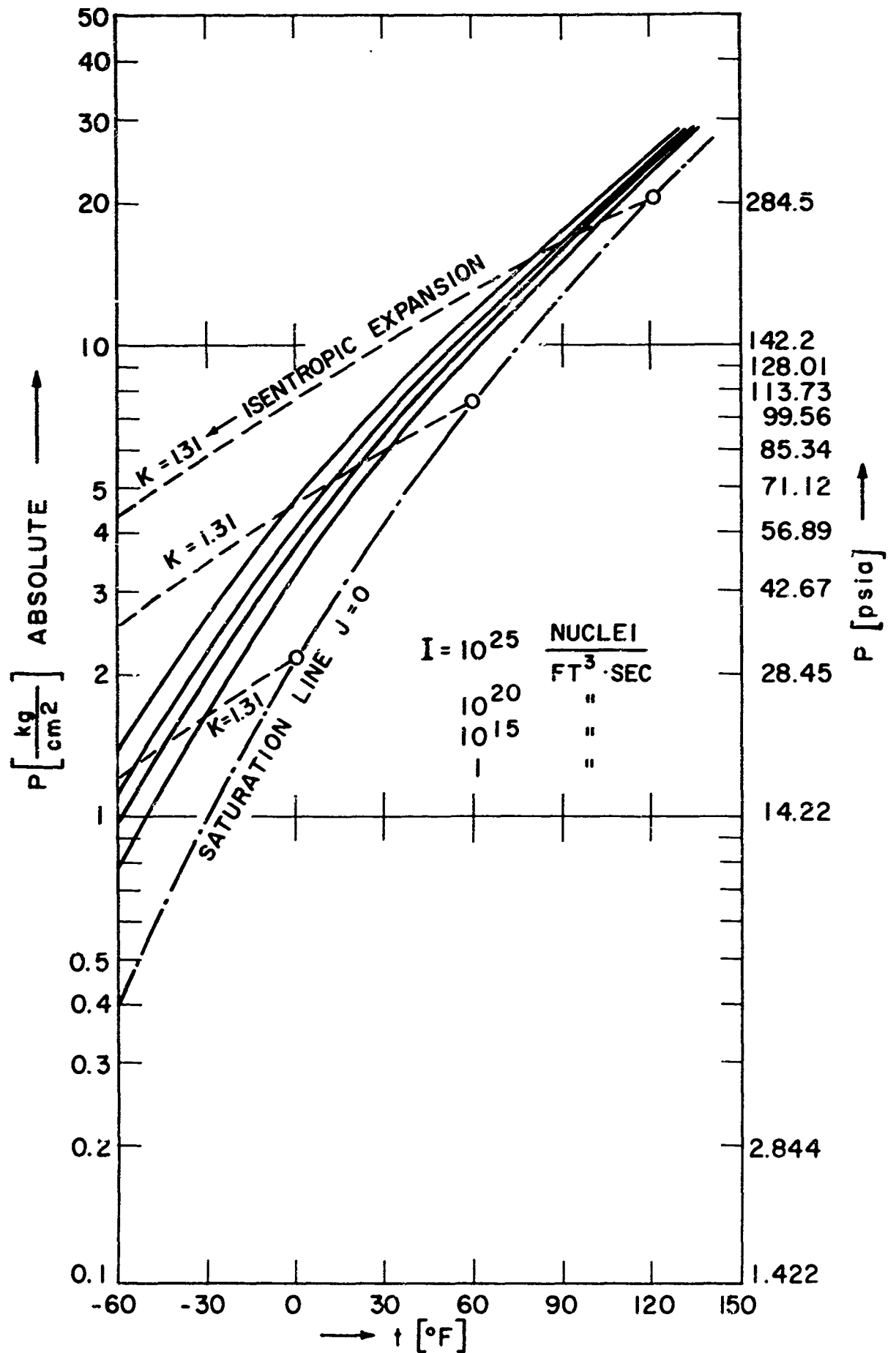FIG 18 ILLUSTRATES UNSTEADINESS NEAR NOZZLE THROAT AT HIGH R_e's
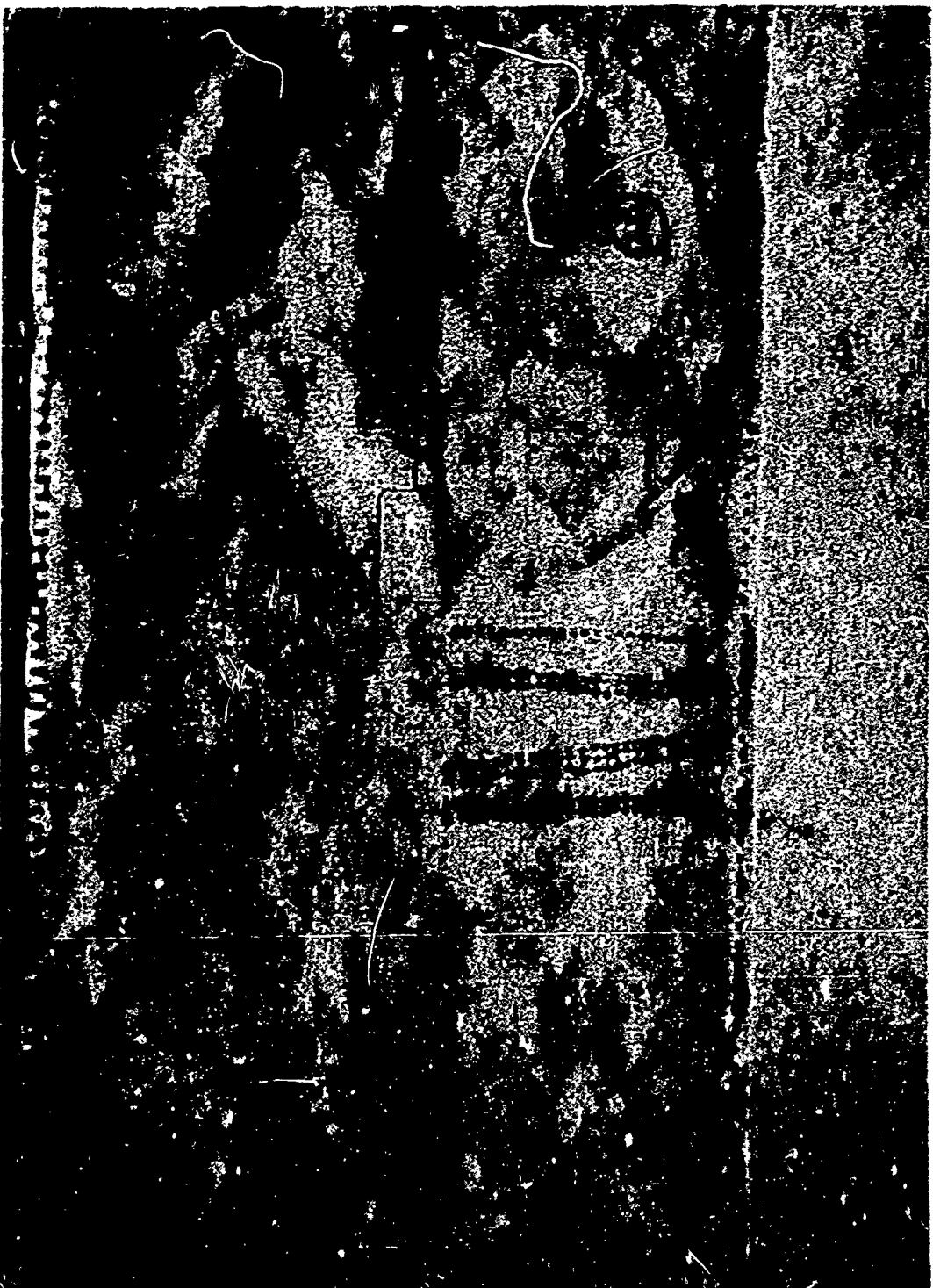
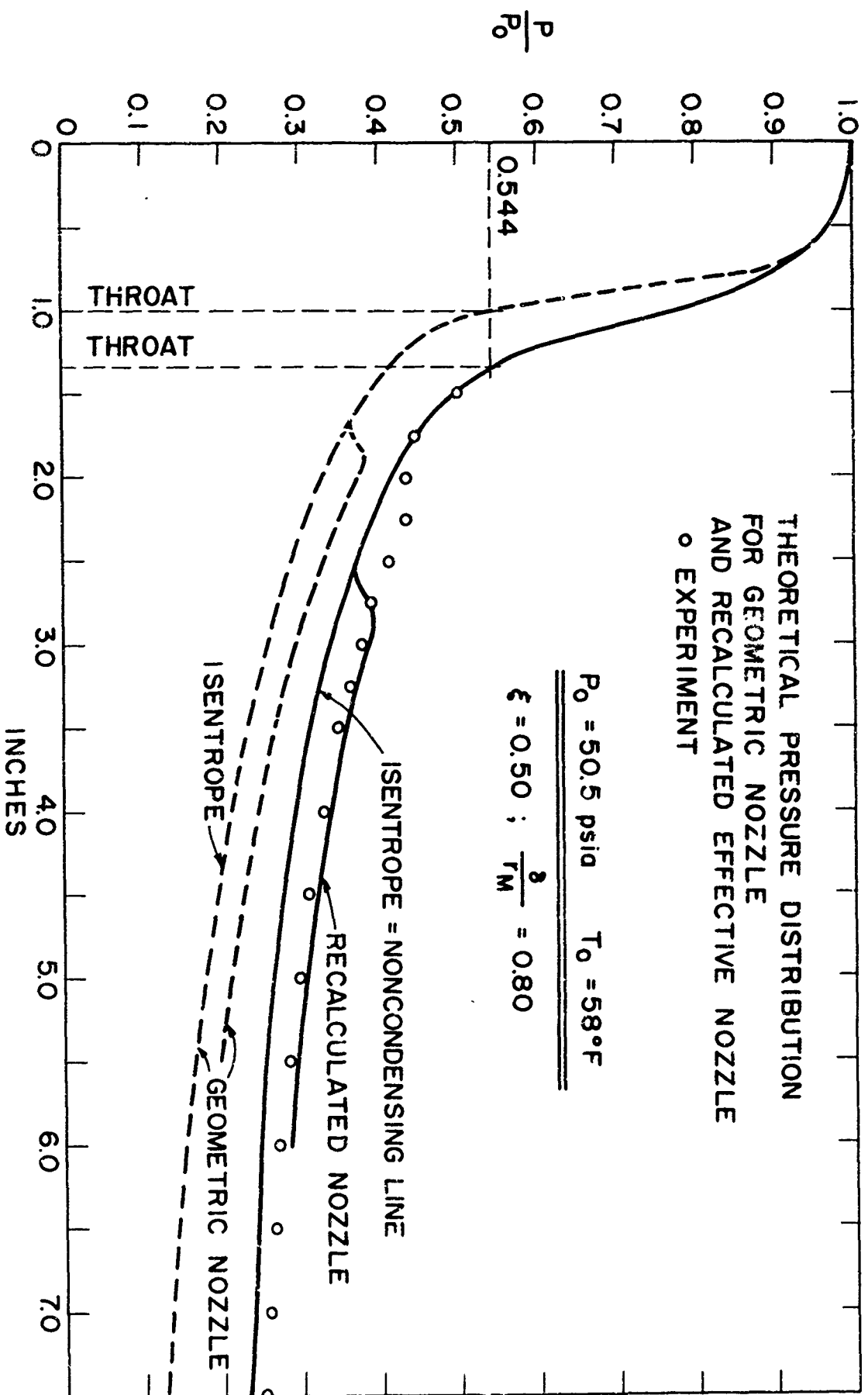FIG. 19 LINES OF CONSTANT NUCLEATION RATE, I
FOR NH_3

FIG. 20 THEORETICAL PRESSURE DISTRIBUTION FOR GEOMETRIC NOZZLE AND
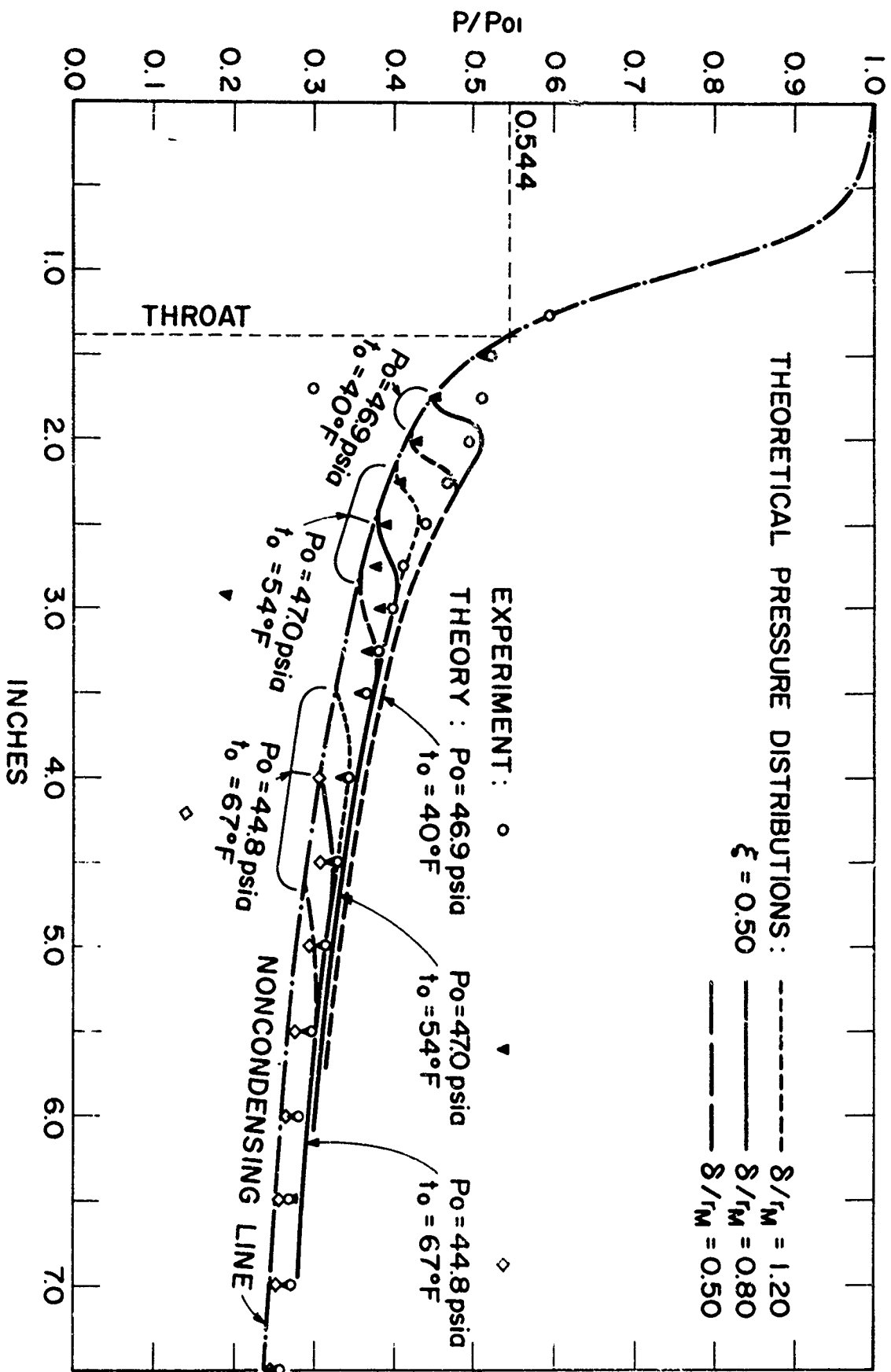RECALCULATED EFFECTIVE NOZZLE

FIG. 21A EFFECT OF CORRECTION OF SURFACE TENSION ON THEORETICAL PRESSURE DISTRIBUTION
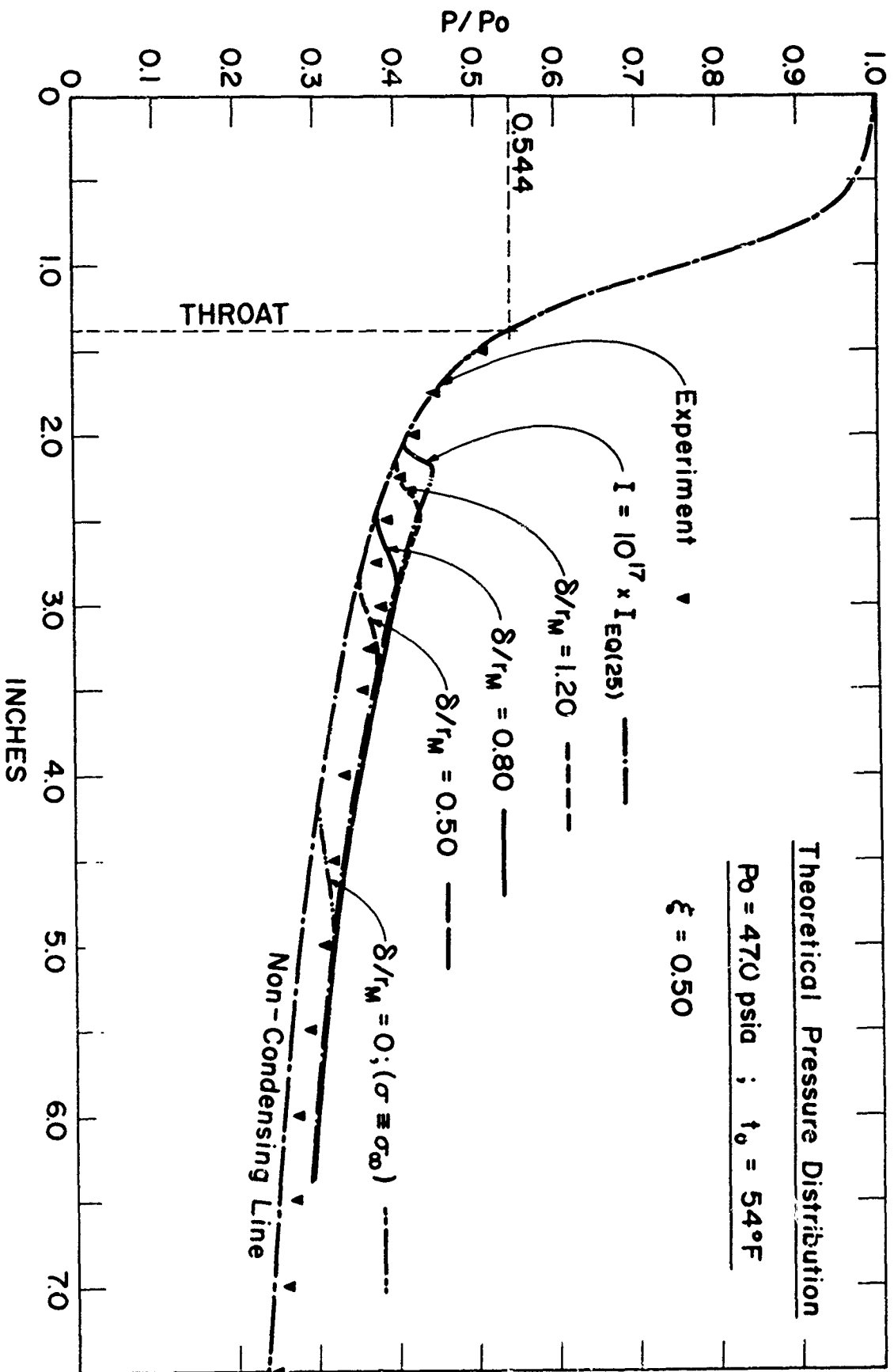
FIG. 21B EFFECT OF VARIATION IN NUCLEATION RATE I ON THEORETICAL PRESSURE DISTRIBUTION
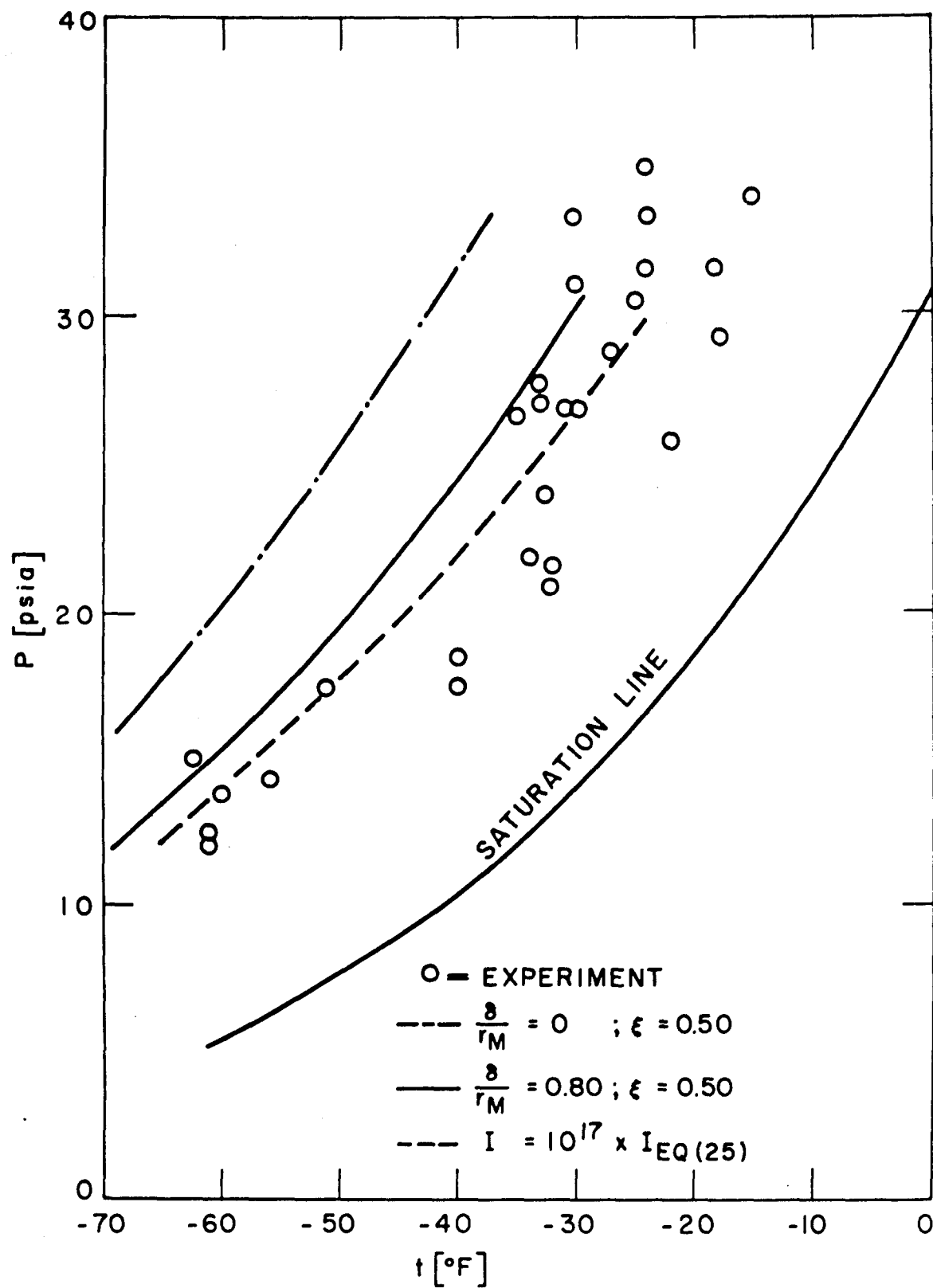
P/Po

0.544

THROAT

Experiment ▼

$I = 10^{17} \times I_{EQ(25)}$ ——

$\delta/r_M = 1.20$ —— —

$\delta/r_M = 0.80$ ——

$\delta/r_M = 0.50$ ——

$\delta/r_M = 0; (\sigma \equiv \sigma_\infty)$ —— —

Non-Condensing Line

Theoretical Pressure Distribution

Po = 47.0 psia ; t_o = 54°F

ξ = 0.50

INCHES

FIG. 22 INCIDENCE OF CONDENSATION IN PRESSURE –
TEMPERATURE –DIAGRAM.